GF Instruments, s.r.o.
Geophysical Equipment and Services

Short guide for electromagnetic conductivity mapping and tomography

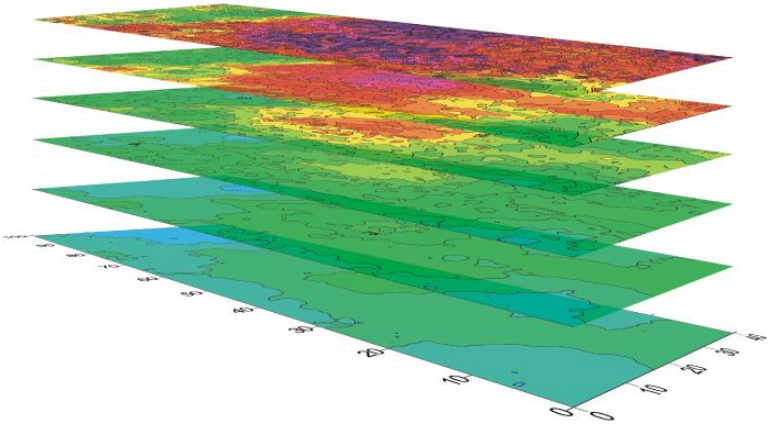

Address of the manufacturer:

GF Instruments, s.r.o.
Purkyňova 144
61200 Brno

tel: +420 549 522 919
fax: +420 549 522 915
e-mail: info@gfinstruments.cz
www: http://www.gfinstruments.cz

Edition 2016

GF Instruments, s.r.o.
Geophysical Equipment and Services

Short guide for electromagnetic conductivity mapping and tomography

This guide brings a brief description of geophysical and technical features of the electromagnetic method accompanied with illustrative examples of multilayer mapping and profiling. However, this new edition is completed by rather complex physical theory useful both for academic sphere and for skilled users. You can find this chapter at the end of the brochure.

Chapter 1
General features, depth range and resolution

The most important advantage of electromagnetic conductivity meters is fast contactless mapping of apparent conductivity and inphase with possibility of EM inversion (section imaging) if several layers are measured together.
While talking about true conductivity meters it is necessary to take care especially of their three crucial properties:

- short & long term stability of readings (negligible temperature drift, no need of frequent recalibration)
- correct absolute calibration of apparent conductivity
- defined depth range.

Stability of reading is determined by design quality of electronics and mechanical parts of the device. Correct calibration depends on the quality (structure homogeneity) and proper conductivity level of calibrating places. Depth range is determined by the distance of magnetic dipoles (distance between coil centers of transmitter and receiver).

Keeping the above mentioned instrument features we can obtain quick and useful results that match very well with DC resistivity methods (maps, slices and sections from 2D and 3D tomography). EM measurement could be easily performed on dry or frozen ground as the method is contactless.

The pictures below show normalized sensitivity function for all CMD instruments. (The depth means depth under the probe.) For instance CMD 4 in high depth range is the most sensitive for object 1.3 m under the probe. Effective depth (where 75% of cumulative sensitivity is achieved) is 6 m. Formulae for calculation of normalized sensitivity are introduced in the theoretical chapter at the end of the brochure.

Sensitivity functions for high and low depth range:

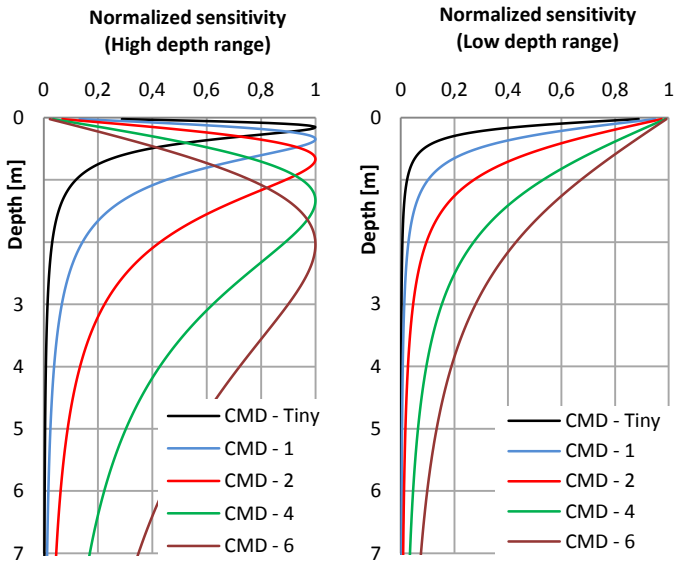

GF Instruments, s.r.o.
Geophysical Equipment and Services

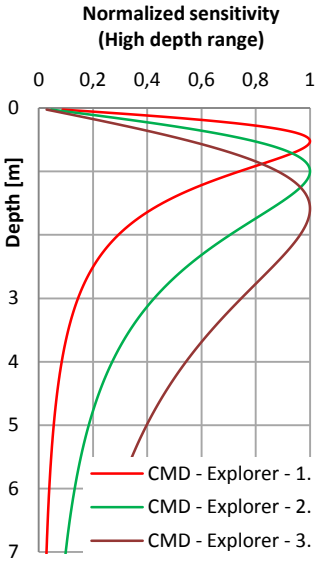

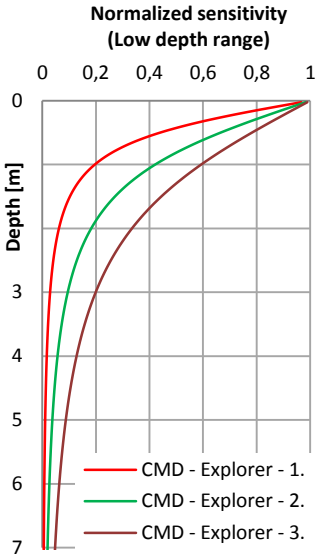

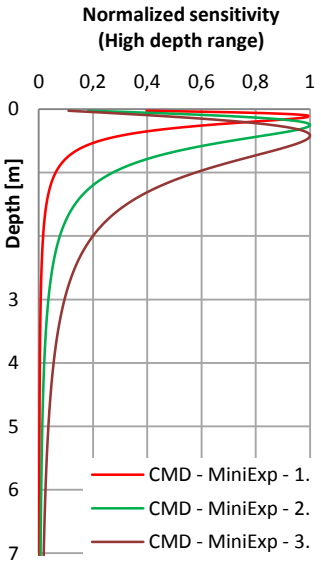

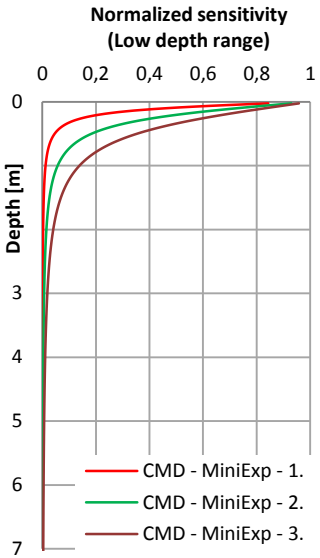

GF Instruments, s.r.o.
Geophysical Equipment and Services

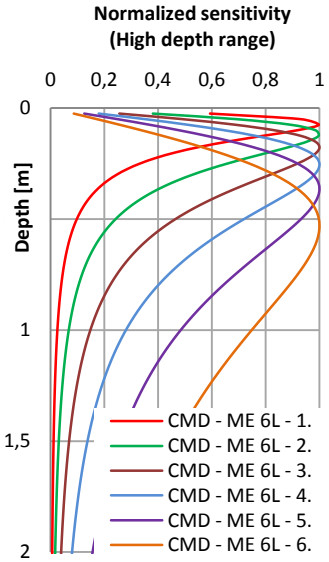

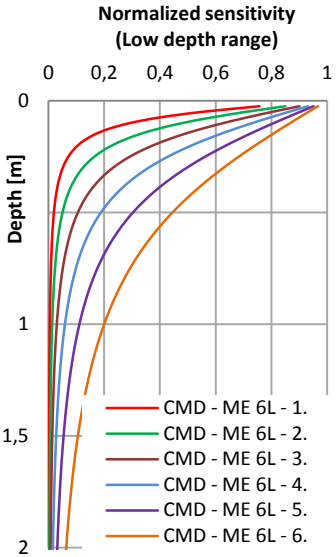

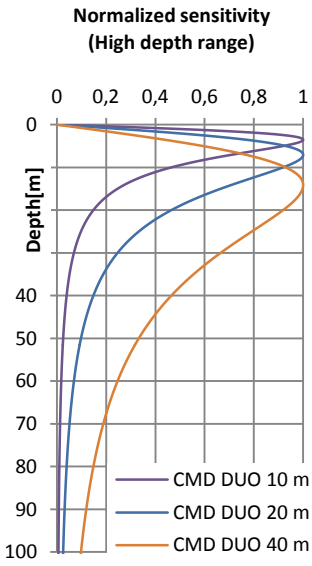

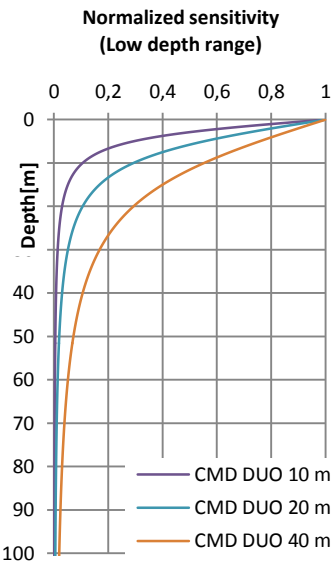

There are two basic ways how to provide requested measuring depth range – by the choice of dipole distance (distances) or by the change of the orientation of dipoles (from vertical to horizontal direction). The first one is more convenient especially if EM inversion is calculated from multilayered measurement. The second one (leading approximately to half depth range) is auxiliary but useful for fast judgment of structure when only one single depth probe is available.

Resolution and depth range are closely related. Increasing depth range decreases resolution and vice versa. Resolution can be significantly improved by EM inversion which improves depth and size imaging of objects in slices and sections as well.

Inphase quantity

The second parameter which is measured simultaneously with apparent conductivity is inphase. It is defined as relative quantity in ppt (part per thousand) of primary magnetic field and is closely related to magnetic susceptibility of measured material. The inphase can especially serve for indication of artificial metal objects like cables, pipes, reinforced concrete, tanks etc. Thus the inphase map can help to distinguish artificial structures from natural geology seen in apparent conductivity map.

GF Instruments, s.r.o.
Geophysical Equipment and Services

EM inversion

EM inversion serves for data processing at multilayer measurement. Although the EM inversion never gives so detailed and accurate results as DC resistivity processing, its useful contribution is obvious for many cases of investigation. Together with apparent conductivity and resistivity maps from individual depths, EM inversion brings quick and complex view on the studied structure.

There are two typical ways of EM inversion – with sudden or fluent change of conductivity/resistivity in calculated inverse model. The up-to-date choice of commercially available EM inversion software for shallow depth range conductivity meters is really not wide.
For CMD data processing we offer three ways of inversion:

- CMD-Explorer system (for 2 layered model – structure with sudden conductivity/resistivity change).
  1D inversion is made either directly in field during measurement (control unit shows upper layer conductivity, bottom layer conductivity and depth of their border) or as post processing by CMD PC software with output of section for Surfer.
- IX1D by Interpex (especially suitable for structures with sudden conductivity change).
  1D inversion in conductivity section can be processed either automatically or manually (with starting model and individual spot processing).
- Res2Dinv and Res3Dinv by Geotomo (convenient for structures with fluent resistivity change).
  2D and 3D inversions with output of resistivity sections and slices use transformed EM data (features similar to DC pole-pole array) exported from CMD PC software.

For the possibility of effective EM inversion a measurement with CMD-Explorer, CMD-Mini Explorer or CMD-Mini Explorer 6L is recommended. Inversion from a combination of both vertical and horizontal (Hi/Lo) measurement is not considered as a general improvement of model section.

The choice of the data processing method is a crucial point of good geophysical interpretation. There is no major general purpose processing method for EM data. For proper decision we recommend to take in consideration the preliminary idea of investigated structure and the goal of survey with the respect to your familiarity with interpretation software.
For basic tasks primary apparent conductivity/resistivity maps are quite sufficient. For advanced user there is a number of ways of data processing (including EM inversion) shown in Chapter 2.

Following Comparisons of Model Resistivity Sections by Res2Dinv show 2D inversion of DC and EM data from the same lines. First two pictures confirm good accordance of the border shape and resistivity values. The CMD-Explorer measurement with low depth range matches better with real border depth and thus gives more realistic result than the measurement with high depth range. On the other side the CMD-MiniExplorer on the same structure (next picture) gives better results with high depth range than with low depth range due to the same reason. The last Comparison obtained from CMD-MiniExplorer 6L shows both good border evaluation with high depth range and better detection of surface anomalies with low depth range.

Comparison of Model Resistivity Sections by Res2Dinv

GF Instruments, s.r.o.
Geophysical Equipment and Services

DC measurement with ARES (Schlumberger array, 48 electrodes, 1 m spacing)

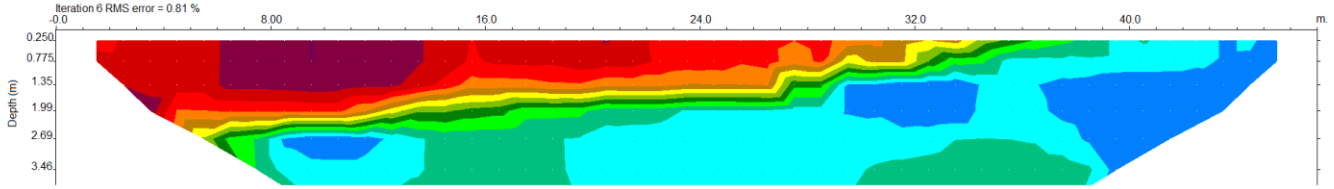

EM measurement with CMD-Explorer (high depth range)

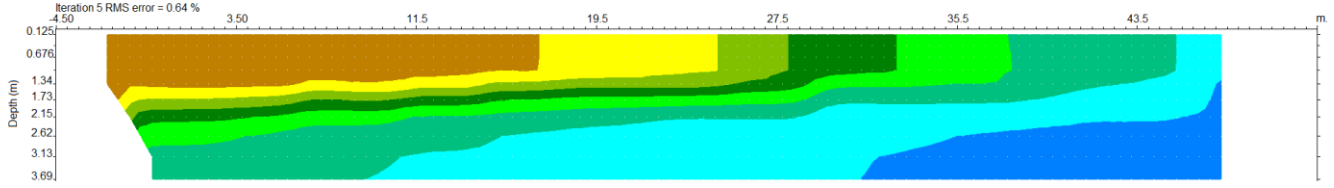

EM measurement with CMD-Explorer (low depth range)

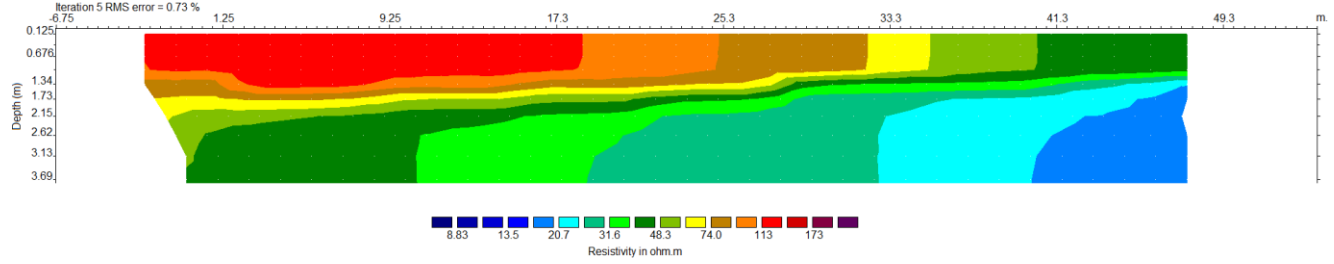

Comparison of Model Resistivity Sections by Res2Dinv

GF Instruments, s.r.o.
Geophysical Equipment and Services

DC measurement with ARES (Schlumberger array, 48 electrodes, 0.5 m spacing)

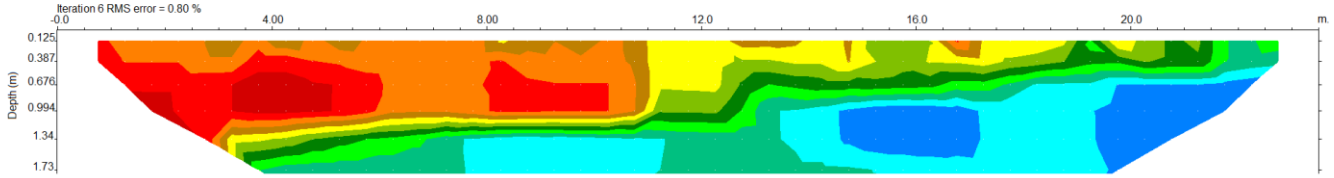

EM measurement with CMD-MiniExplorer (high depth range)

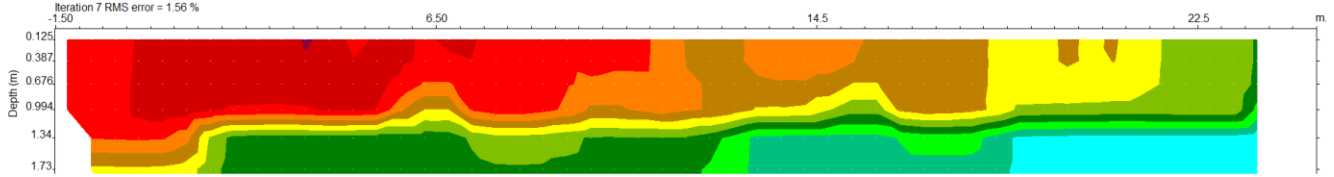

EM measurement with CMD-MiniExplorer (low depth range)

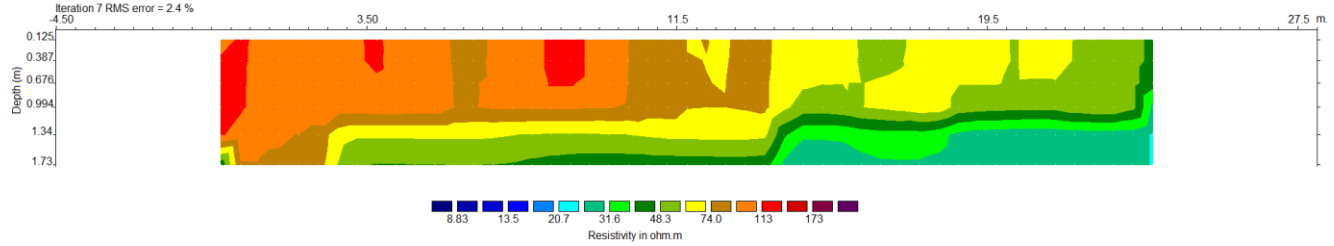

Comparison of Model Resistivity Sections by Res2Dinv

GF Instruments, s.r.o.
Geophysical Equipment and Services

DC measurement with ARES (Schlumberger array, 48 electrodes, 0.5 m spacing)

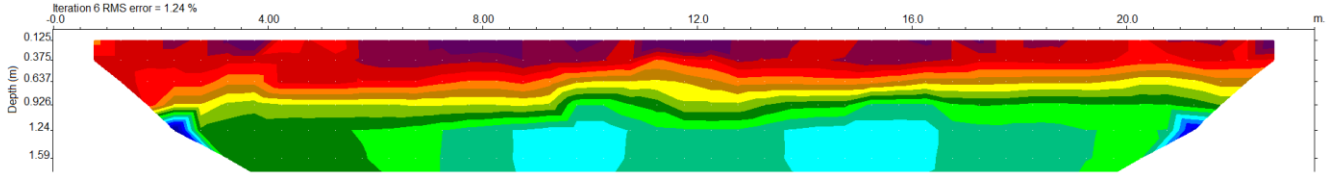

EM measurement with CMD-ME 6L (high depth range)

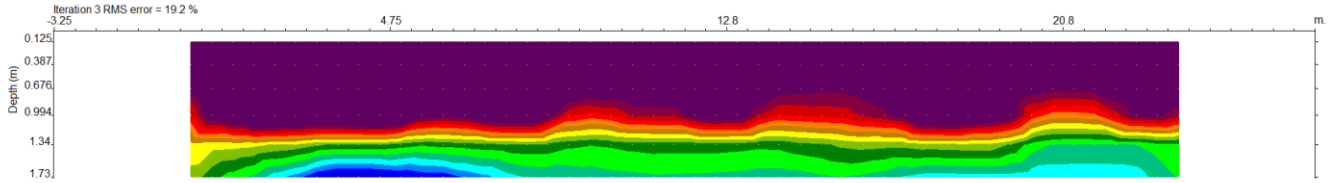

EM measurement with CMD-ME 6L (low depth range)

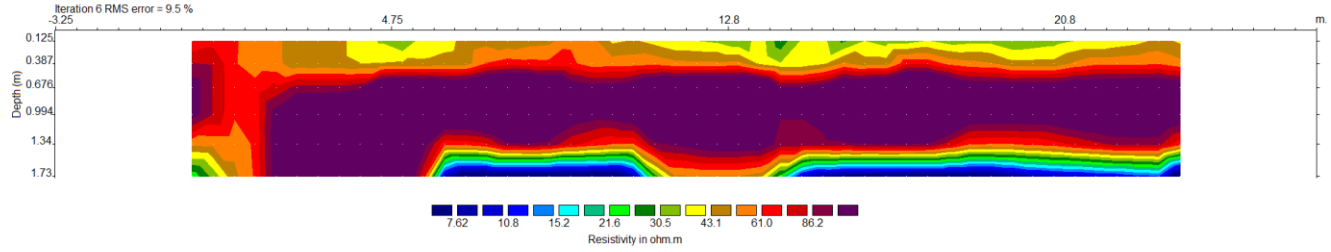

GF Instruments, s.r.o.
Geophysical Equipment and Services

Multidepth measurement - wish and reality regarding use of different frequencies

It would be really great to obtain correct conductivity maps from many different depths using broad band antennas with stable transmitter to receiver distance and various frequencies of EM field. Unfortunately, physics does not support such a possibility:
For correct conductivity measurement we have to remain at low induction numbers. Thus the effective depth range is determined by dipole center distance. The choice of frequency (in a limited range) can serve only for tuning of the shape of the calibration curve and for cancellation of external EM interferences.

We will find two basic effects of multifrequency measurement with constant dipole center distance:

- The frequency is changing from hundreds of Hz to 100 kHz approximately so the device remains usually at low induction number. We will find the depth range determined by the distance of magnetic dipoles and conductivity maps mostly show no frequency depending differences. Influence of broadband antennas decrease sensitivity and stability of measuring system.
- The frequency change is bigger (e.g. to 1 MHz). The measuring device is usually crossing the transient zone of induction numbers with ambiguous response and declining calibration curve with the depth range influenced by conductivity and by frequency at the same time. Measured results cannot be correctly calibrated in conductivity and consequently used for EM inversion.

Following pictures from the same testing area illustrate how the resistivity map changes if we change the frequency only and if we change the dipole distance. The accompanying DC resistivity section shows detailed structure on the same place.

GF Instruments, s.r.o.
Geophysical Equipment and Services

Apparent resistivity maps measured with various frequencies and 2 m dipole distance

All maps show approximately the same results without obvious relation to the real depth structure.

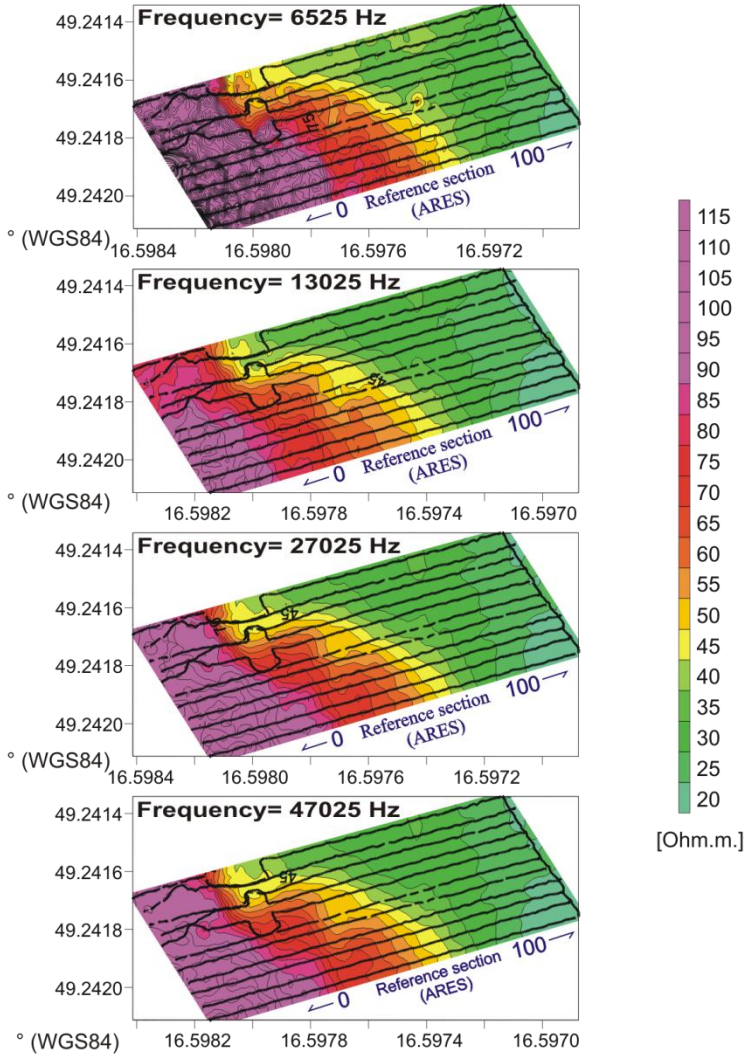

GF Instruments, s.r.o.
Geophysical Equipment and Services

Apparent resistivity maps measured with CMD-1, CMD-2 and CMD-4 probes

The map from CMD-1 shows generally higher resistivity being influenced mostly by upper resistive layer (see DC section). The maps from CMD-2 and CMD-4 show proportionally lower resistivities due to the more and more significant contribution of the clayey layer at approx. 5 m depth.

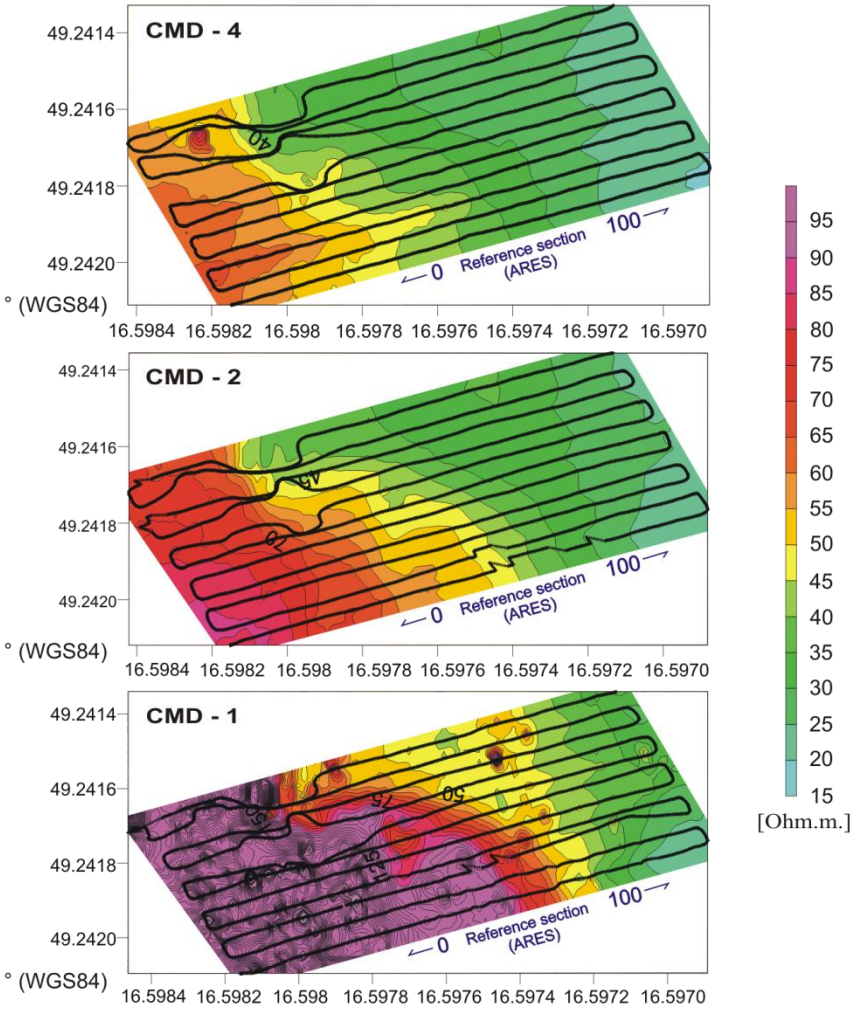

GF Instruments, s.r.o.
Geophysical Equipment and Services

Reference section measured by DC method with ARES system

The section shows structure with bottom clayey layer (conductive) covered with quaternary sediments (sand and gravel). The upper resistive layer is regularly pinching from position 0 to approximately position 60.

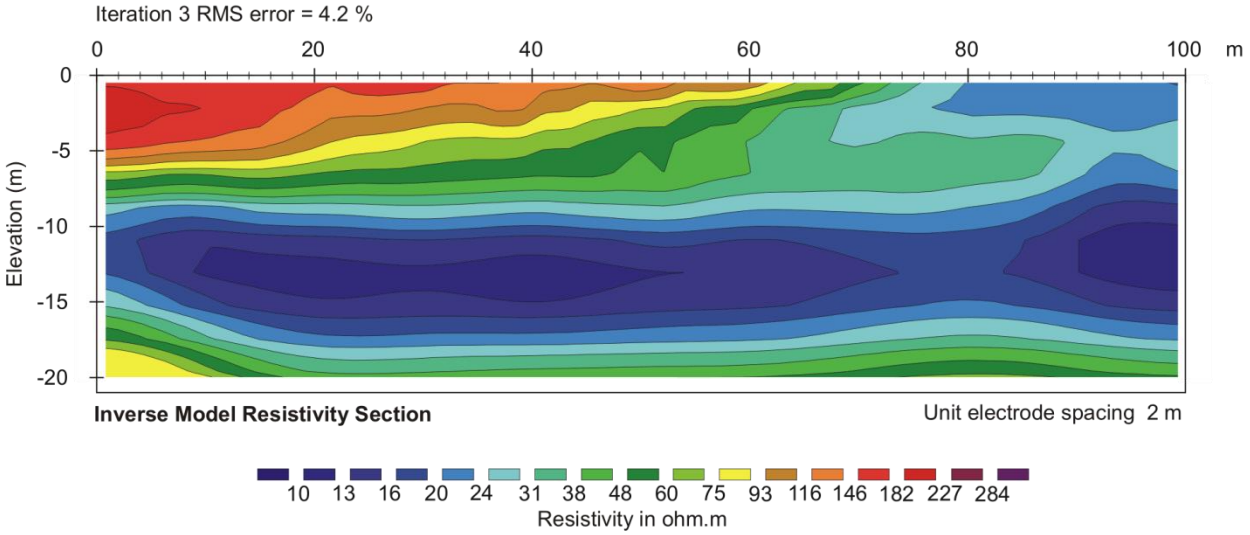

GF Instruments, s.r.o.
Geophysical Equipment and Services

Choice of the probe

Eight standard probes are offered covering all typical tasks of shallow EM survey,

CMD-Explorer with simultaneous 6.7 m, 4.2 m, 2.2 m full depth ranges is designed for investigation of layered structures in the frame of geological, geotechnical, prospecting and other tasks. Rich current graphical output (with in-situ inversion) and support of consequent data processing (mapping, sections and inversion) make Explorer ideal for fast and complex EM survey.

CMD-Mini Explorer with simultaneous 0.5 m, 1.0 m, 1.8 m full depth ranges is designed for investigation of very shallow layered structures in the frame of agriculture, forestry, archaeology, road inspection and other tasks. Rich current graphical output (with in-situ inversion) and support of consequent data processing (mapping, sections and inversion) make Mini Explorer ideal for fast and complex EM survey.

CMD-DUO two men operated with variable 15/30/60 m full depth range (dipole distance of 10/20/40 m) is useful for distinguishing of deeper situated geological structures as bedrock, weathered zones, cavities and fissures.

CMD-4/6 with variable 6/9 m full depth range allows measurement with the same or extended depth range as classic CMD-4 in the frame of its typical applications.

CMD-4 with 6 m full depth range and typical use in geological and environmental survey can be used for many connected tasks like mapping of raw material deposits, watered zones,

localization of waste dumps, buried tanks and other hidden objects.

CMD-2 with 3 m full depth range and typical use in engineering survey can serve for cable and pipe localization as well as for general assessment of construction site (e.g. detailed investigation of basement positions – clayey, sandy, rocky parts).

CMD-1 with 1.5 m full depth range is typically used in archaeology and agriculture.
This probe carried mostly near the ground surface allows detailed distinguishing of buried objects (vertically orientated zones, e.g. basement of walls, rock outcrops) and conductivity assessment of upper thin layers.

CMD-Tiny with 0.7 m full depth range allows the highest resolution of shallow situated objects in the frame of monitoring of artificial structures (roads, buildings, historical sites) as well as soil quality evaluation in agriculture and forestry.

Special probes with up to 10 m dipole distance and with up to 6 simultaneous receivers are available on request.

CMD-Mini Explorer 6L with simultaneous 0.3 m, 0.5 m, 0.8 m, 1.1 m, 1.6 m, 2.3 m full depth ranges is designed for high resolution investigation of shallow layered structures in the frame of agriculture, forestry, archaeology, criminology, road inspection and civil engineering.

Chapter 2
Examples of multidepth investigation

This chapter shows typical examples from measurement with CMD-Explorer and CMD-MiniExplorer (including 6L). CMD software for PC provides data transformation and export for commonly spread geophysical processing programs for imaging and inversion (Surfer, IX1D, Res2Dinv and Res3Dinv).

Each following part bringing results from a chosen locality begins with reference DC resistivity section measured with ARES instrument that allows a comparison with individual ways of imaging and inversion of EM measurement.

GF Instruments, s.r.o.
Geophysical Equipment and Services

GF Testing Site

The structure is typical with pinching of sandy layer above clayey background.

All available kinds of imaging and inversion are explained here and shown consequently:

- Apparent Resistivity Maps show basic outputs from all three depth graded EM systems of CMD-Explorer.
- Resistivity Slices from EM Inversion by CMD-Explorer show depth graded resistivity maps based on 1D inversion of measured data.
- 2D EM Inversion by CMD-Explorer shows measured apparent resistivity section and inverse model resistivity section based on 1D inversion.
- EM Inversion by IX1D shows conductivity section by Interpex software.
- 2D Imaging and Inversion by Res2Dinv shows measured apparent resistivity section and inverse model resistivity section by Geotomo software.
- 3D Imaging and Inversion by Res3Dinv shows depth graded resistivity slices and resistivity sections along/across measured lines (YZ/XY directions) by Geotomo software.

GF Instruments, s.r.o.
Geophysical Equipment and Services

GF Testing Site
Reference Resistivity Section

Measured with ARES using Schlumberger array

2D imaging and inversion by Res2Dinv

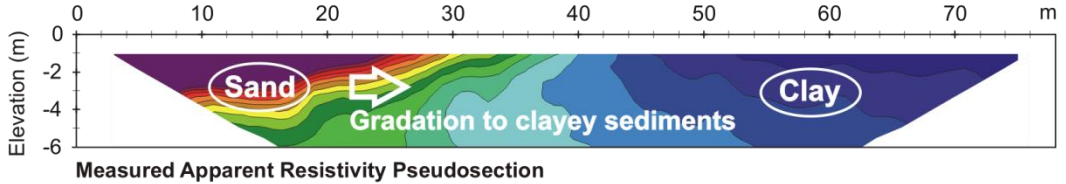

Measured Apparent Resistivity Pseudosection

Iteration 3 RMS error = 1.75 %

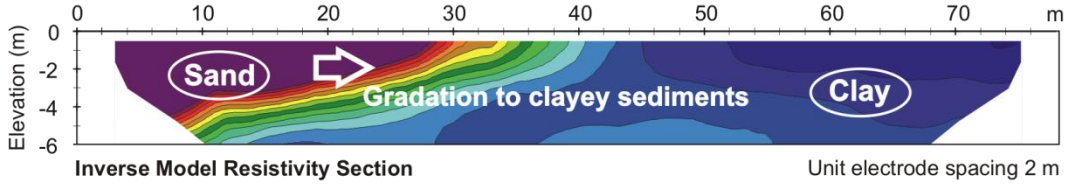

Inverse Model Resistivity Section

Unit electrode spacing 2 m

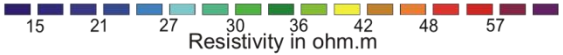

GF Instruments, s.r.o.
Geophysical Equipment and Services

GF Testing Site
Apparent Resistivity Maps

Measured with CMD-Explorer

Imaging by Surfer

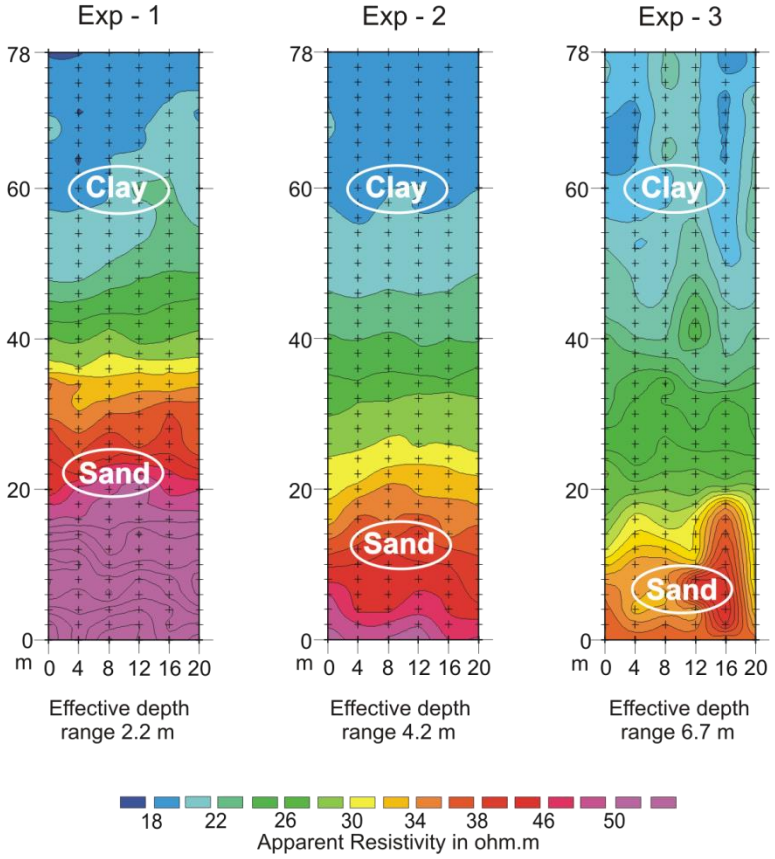

GF Testing Site

Resistivity Slices from EM Inversion by CMD - Explorer

Measured with CMD-Explorer

Imaging by Surfer

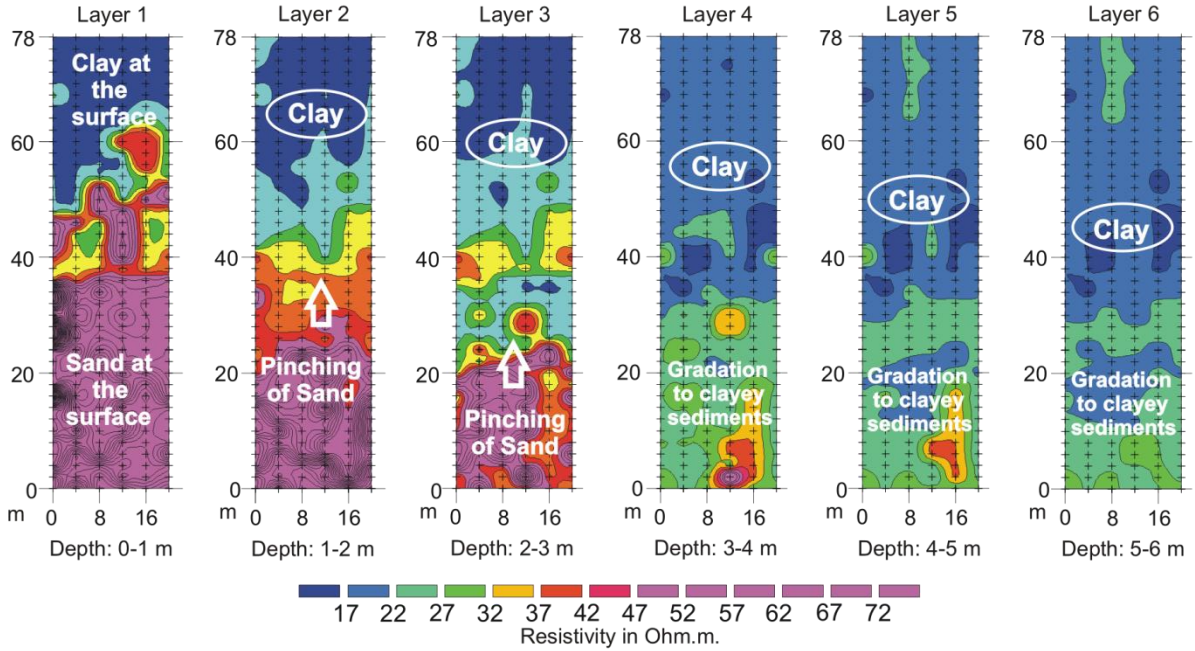

GF Instruments, s.r.o.
Geophysical Equipment and Services

GF Testing Site
2D EM Inversion by CMD-Explorer

Resistivity section measured with CMD-Explorer

Imaging by Surfer

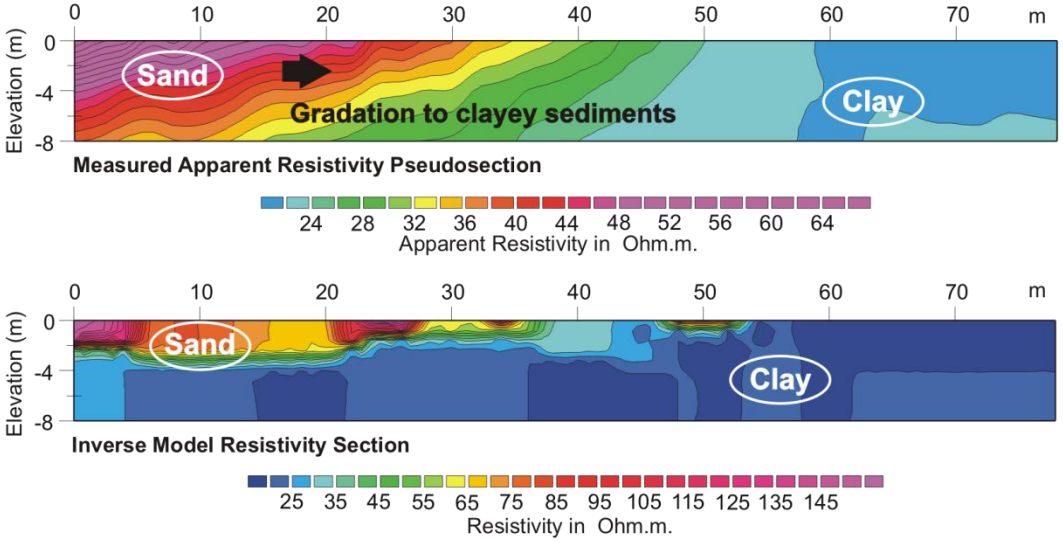

GF Instruments, s.r.o.
Geophysical Equipment and Services

GF Testing Site
EM Inversion by IX1D

Conductivity section measured with CMD-Explorer

Imaging and inversion by IX1D

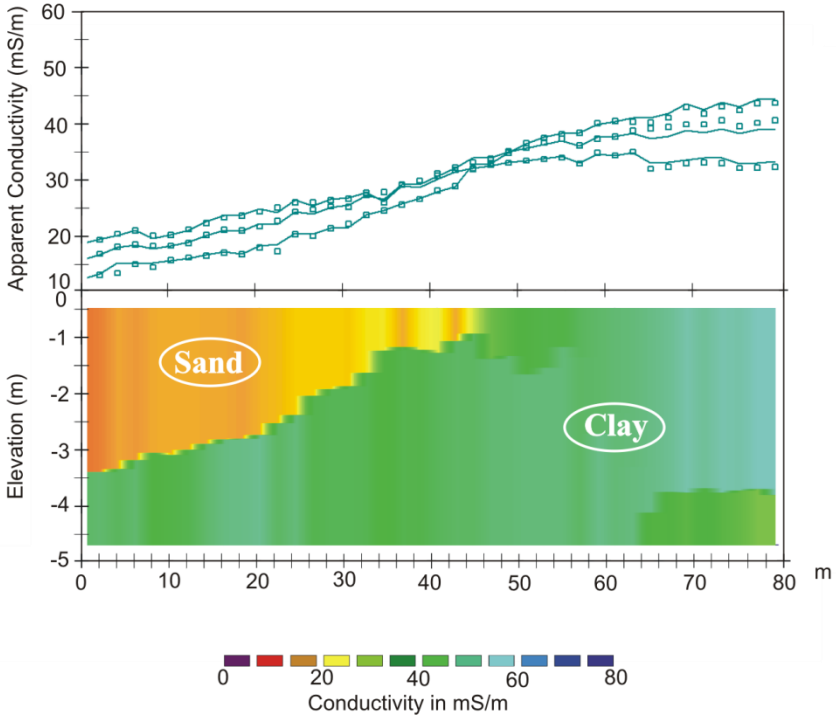

GF Instruments, s.r.o.
Geophysical Equipment and Services

GF Testing Site
2D Imaging and Inversion by Res2Dinv

Resistivity section measured with CMD-Explorer

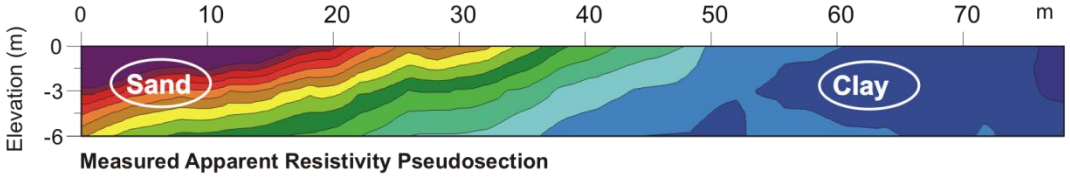

Measured Apparent Resistivity Pseudosection

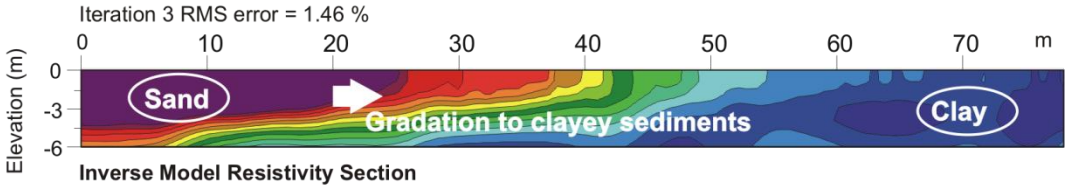

Inverse Model Resistivity Section

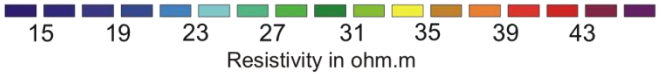

GF Testing Site

3D Imaging and Inversion by Res3Dinv

Resistivity slices measured with CMD-Explorer

Iteration 3 RMS Error = 6.11 %

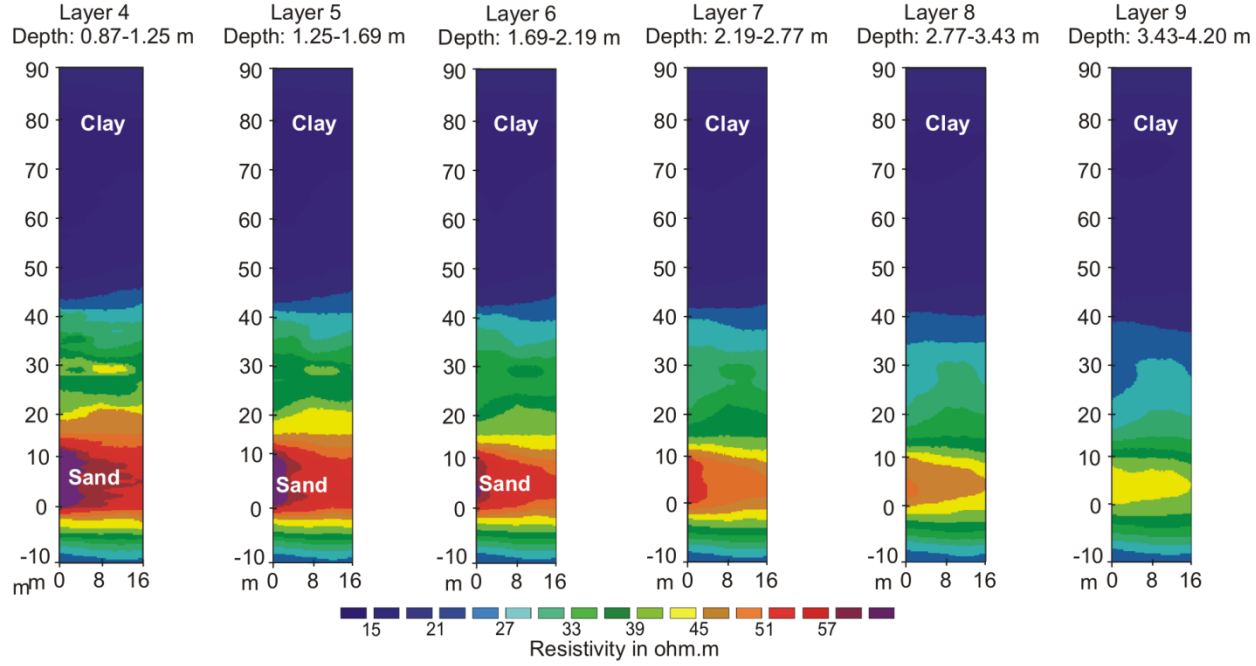

GF Testing Site
3D Imaging and Inversion by Res3Dinv

Resistivity YZ sections measured with CMD-Explorer

Iteration 3 RMS error = 6.11 %

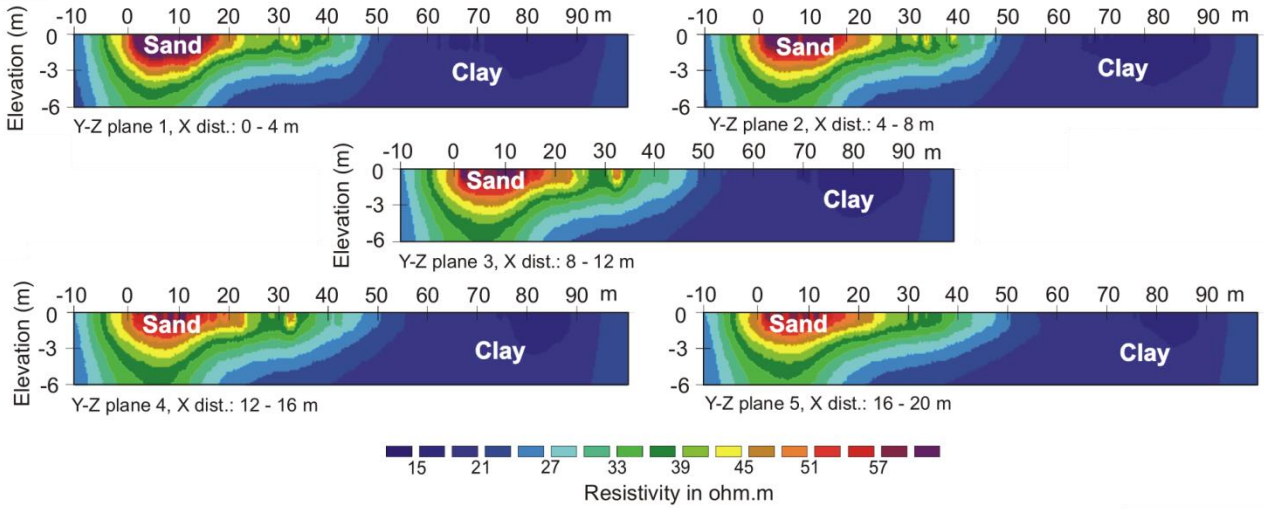

GF Testing Site

3D Imaging and Inversion by Res3Dinv

GF Instruments, s.r.o.
Geophysical Equipment and Services

Resistivity XZ sections measured with CMD-Explorer

Iteration 3 RMS error = 6.11 %

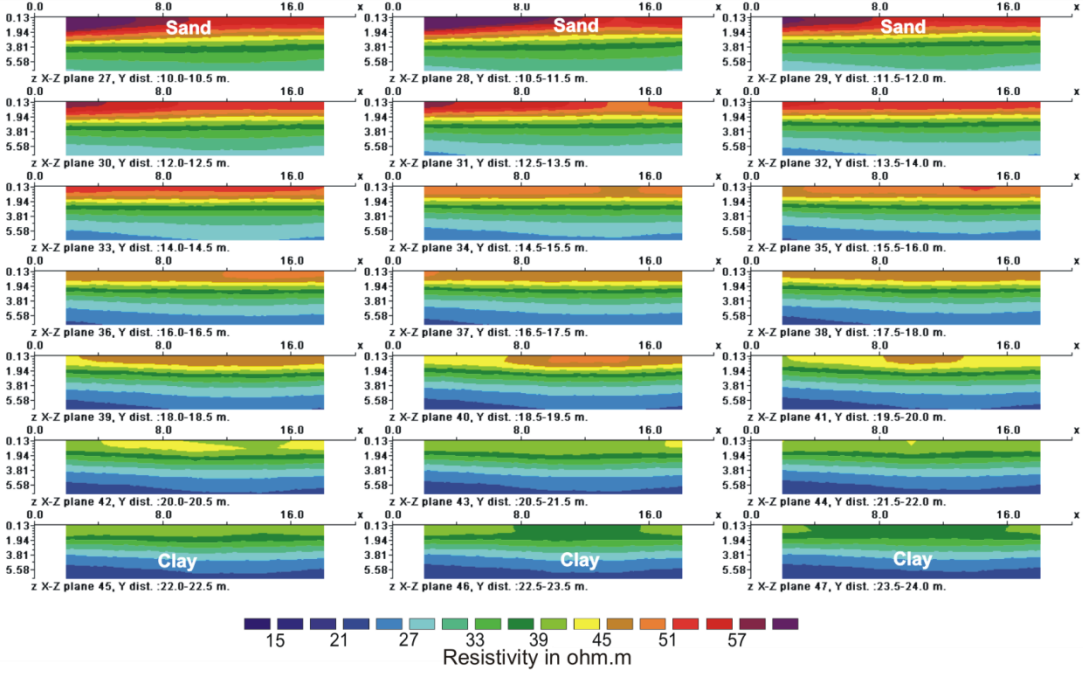

GF Instruments, s.r.o.
Geophysical Equipment and Services

Pinching of Loess Layer

The structure is typical with pinching of loess layer above rocky background.

Chosen kinds of imaging and inversion related to geological structures are shown:

- Apparent Resistivity Maps
- Apparent Resistivity Section
- Conductivity Section from EM inversion by IX1D
- Resistivity Section from 2D inversion by Res2Dinv

Pinching of Loess Layer
Reference Resistivity Section of Geological Structures

Measured with ARES using Schlumberger array

Imaging and inversion by Res2Dinv

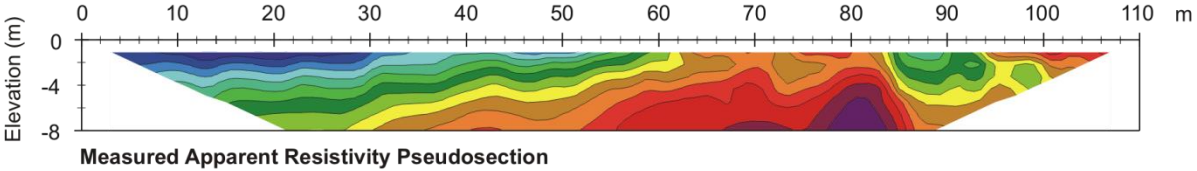

Measured Apparent Resistivity Pseudosection

Iteration 3 RMS error = 2.9 %

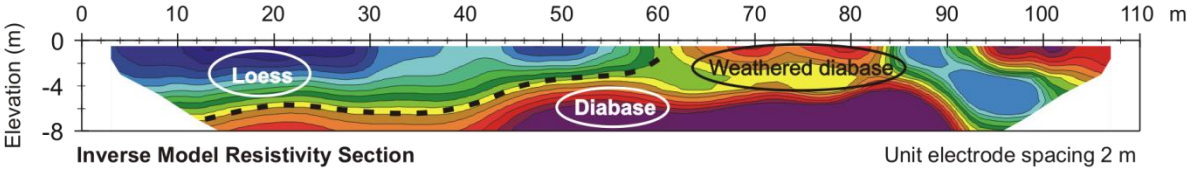

Inverse Model Resistivity Section

Unit electrode spacing 2 m

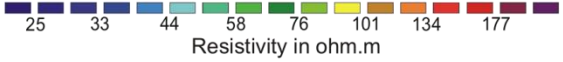

GF Instruments, s.r.o.
Geophysical Equipment and Services

Pinching of Loess Layer

Apparent Resistivity Maps of Geological Structures

Measured with CMD-Explorer

Imaging by Surfer

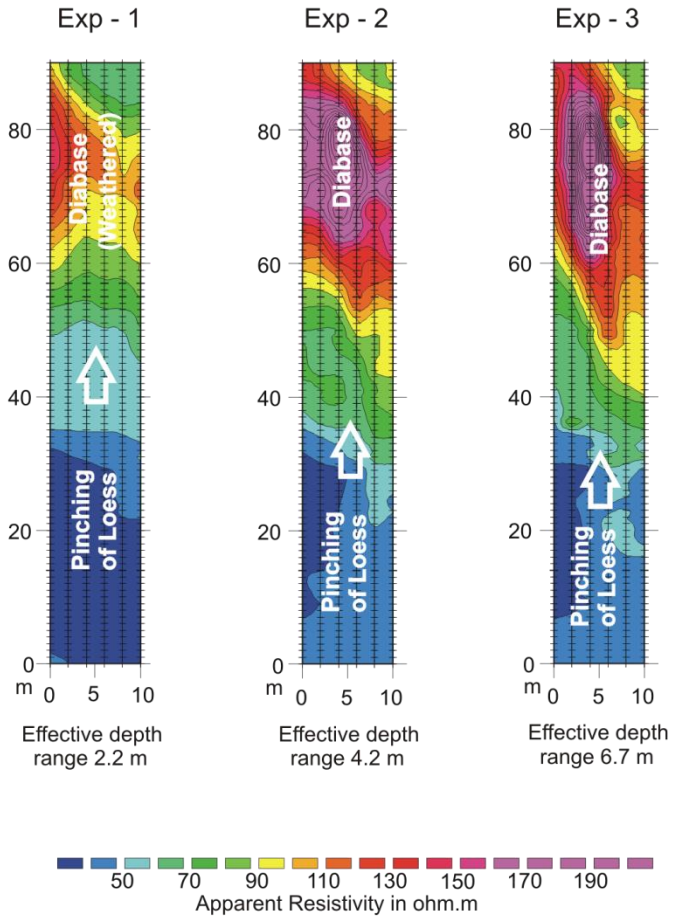

GF Instruments, s.r.o.
Geophysical Equipment and Services

Pinching of Loess Layer

Apparent Resistivity Section of Geological Structures

Measured with CMD-Explorer

Imaging by Surfer

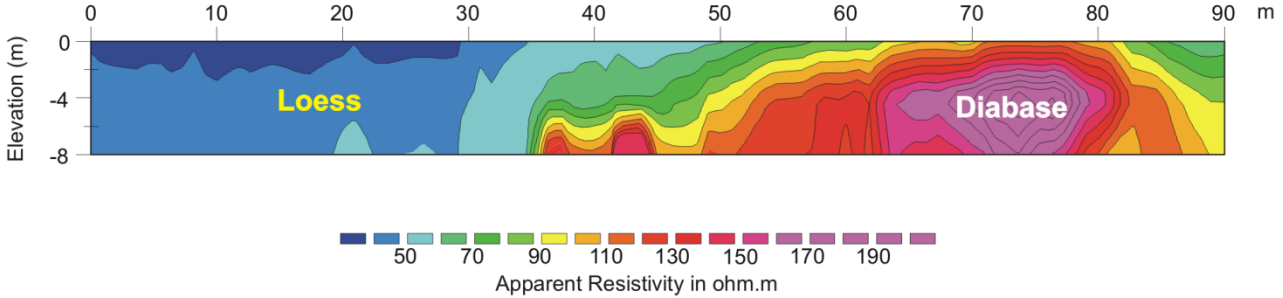

Pinching of Loess Layer
Conductivity Section of Geological Structures

Measured with CMD-Explorer
EM Inversion by IX1D

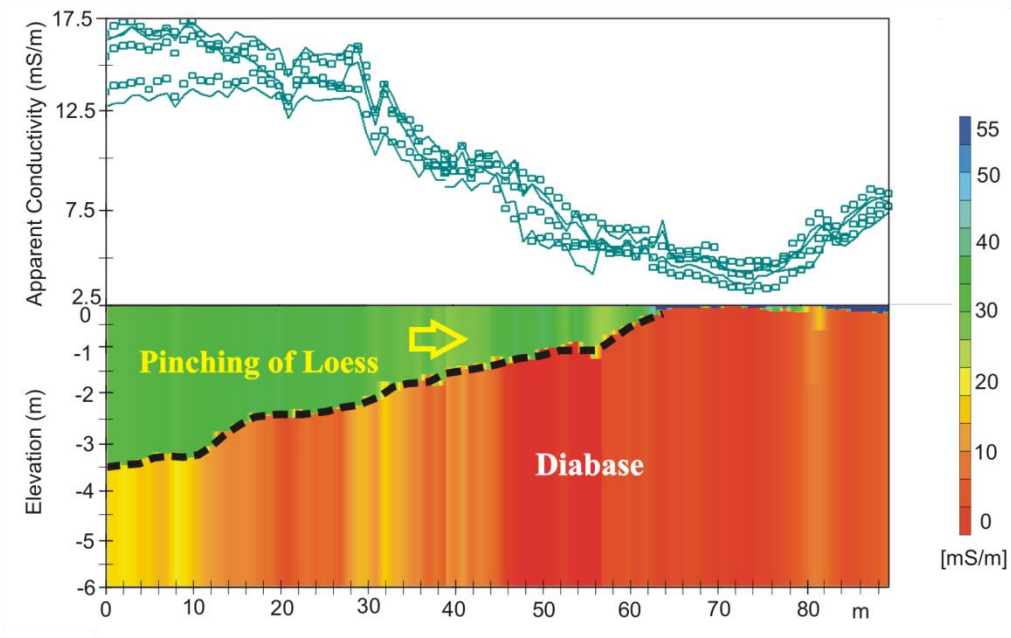

Pinching of Loess Layer
Resistivity Section of Geological Structures

Measured with CMD-Explorer

2D Imaging and Inversion by Res2Dinv

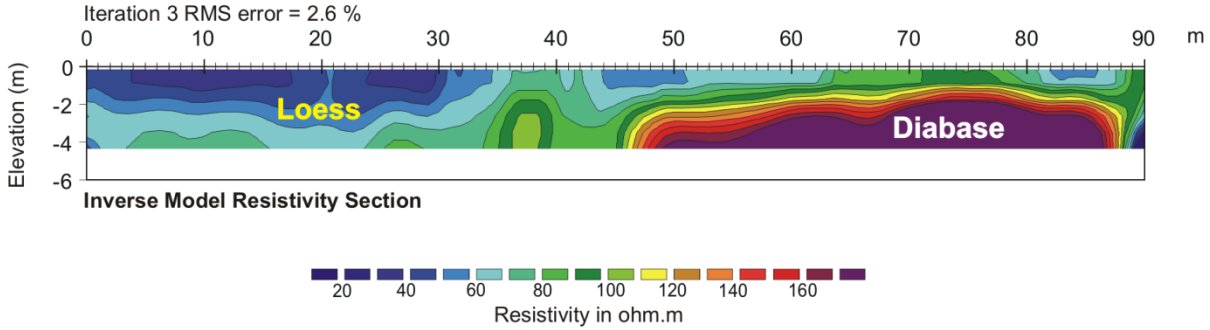

GF Instruments, s.r.o.
Geophysical Equipment and Services

Farming and Woodland Area

Measured area across agricultural land and wood allows studying both geological background (CMD-Explorer) and detailed upper very shallow soil structures (CMD-MiniExplorer).

Chosen useful kinds of imaging and inversion are shown.

Geological structures:

- Apparent Resistivity Maps (confirm well sharp slope of contact with diabase background and sandy loam layer in upper part)
- Resistivity Slices and YZ Sections from 3D Imaging and Inversion by Res3Dinv

Shallow soil structures:

- Apparent Resistivity Maps (with top soil in upper part)
- Apparent Resistivity Section
- Conductivity Section from EM inversion by IX1D
- Resistivity Section with 2D imaging and inversion by Res2Dinv
- Resistivity Slices from 3D inversion by Res3Dinv

Farming and Woodland Area
Reference Resistivity Section of Geological Structures

Measured with ARES using Schlumberger array

2D imaging and inversion by Res2Dinv

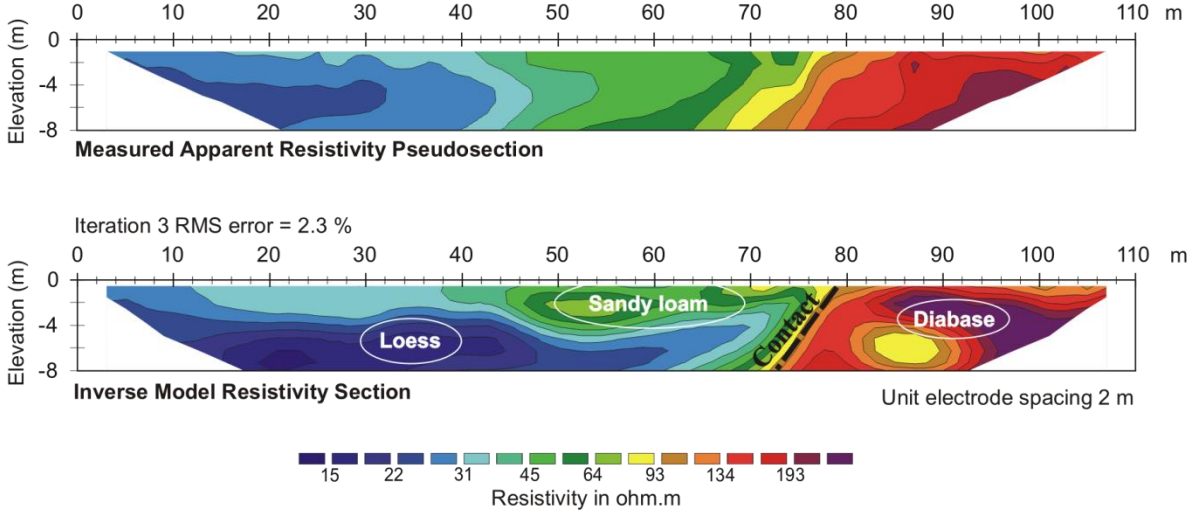

GF Instruments, s.r.o.
Geophysical Equipment and Services

Farming and Woodland Area
Apparent Resistivity Maps of Geological Structures

Measured with CMD-Explorer

Imaging by Surfer

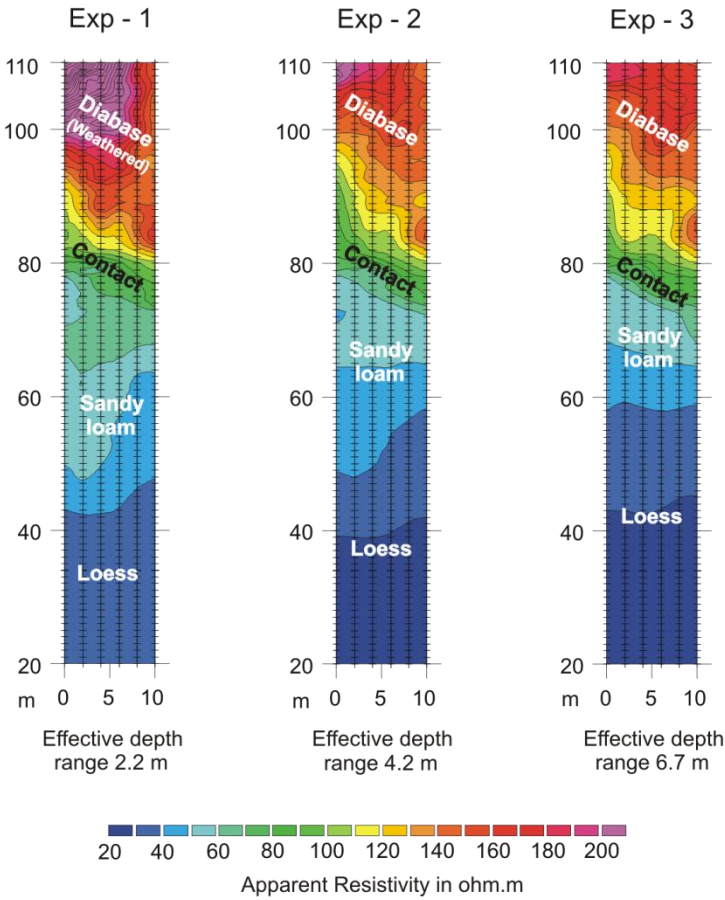

GF Instruments, s.r.o.
Geophysical Equipment and Services

Farming and Woodland Area
Resistivity Slices of Geological Structures

Measured with CMD-Explorer

3D Imaging and Inversion by Res3Dinv

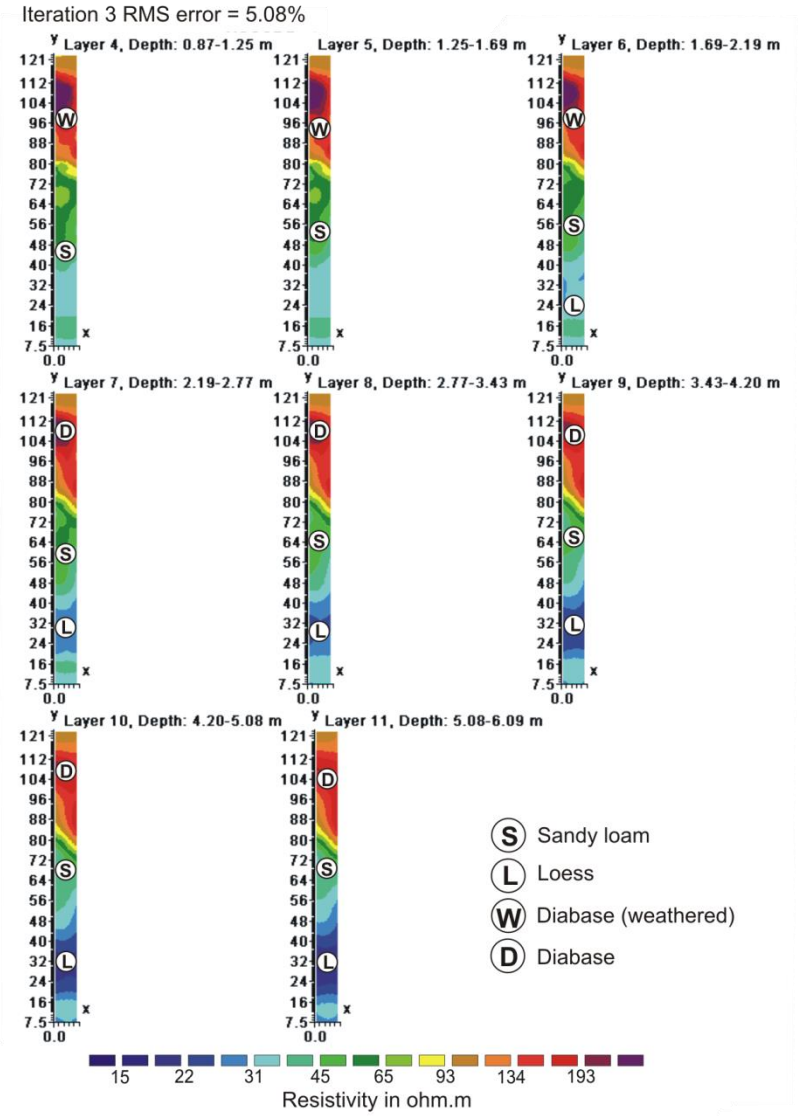

Farming and Woodland Area
Resistivity YZ Sections of Geological Structures

Measured with CMD-Explorer

3D Imaging and Inversion by Res3Dinv

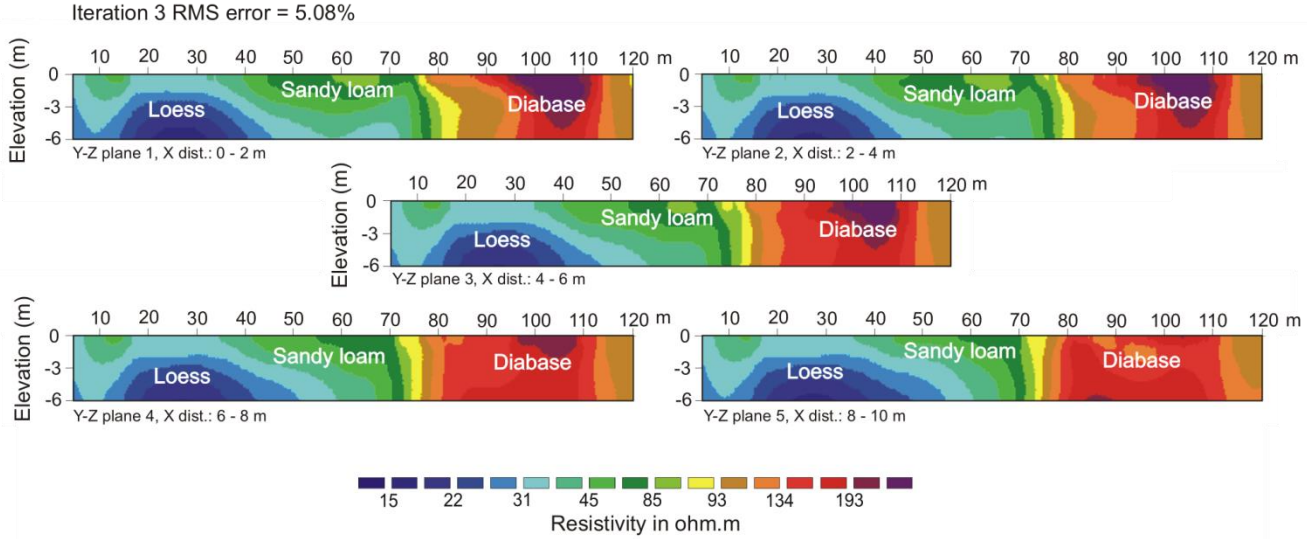

GF Instruments, s.r.o.
Geophysical Equipment and Services

Farming and Woodland Area
Apparent Resistivity Maps of Shallow Soil Structures

Measured with CMD-Mini Explorer

Imaging by Surfer

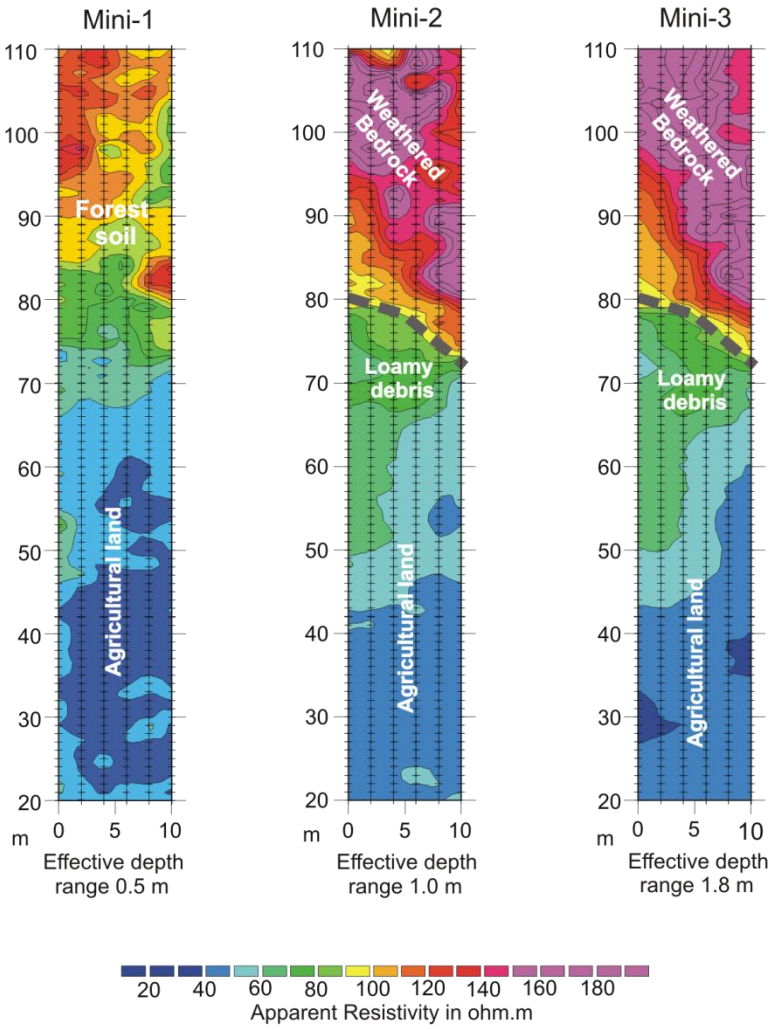

GF Instruments, s.r.o.
Geophysical Equipment and Services

Farming and Woodland Area
Apparent Resistivity Section of Shallow Soil Structures

Measured with CMD-Mini Explorer

Imaging by Surfer

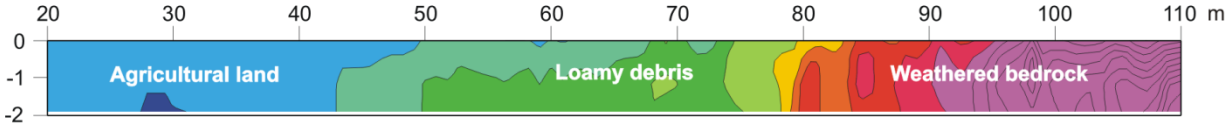

Apparent Resistivity in ohm.m

GF Instruments, s.r.o.
Geophysical Equipment and Services

Farming and Woodland Area
Conductivity Section of Shallow Soil Structures

Measured with CMD-Mini Explorer

EM Inversion by IX1D

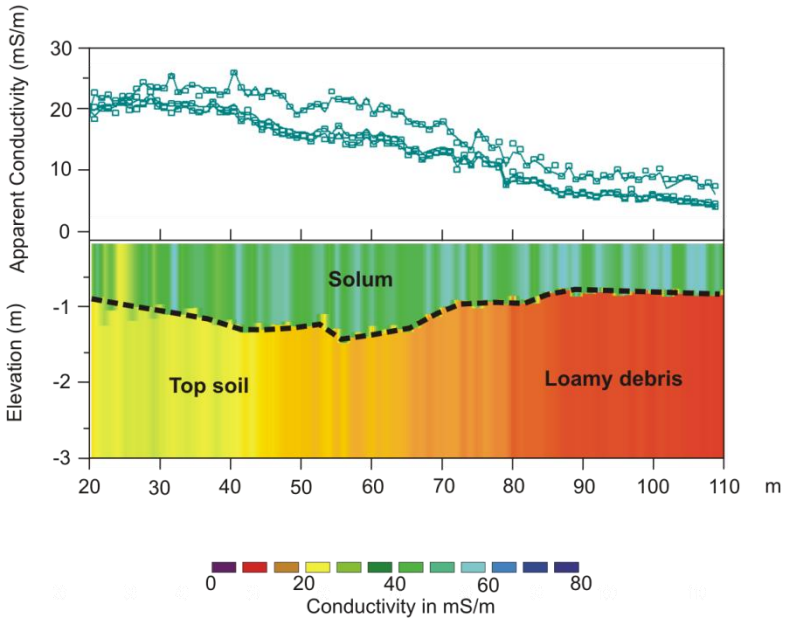

Farming and Woodland Area
Resistivity Section of Shallow Soil Structures

Measured with CMD-Mini Explorer

2D Imaging and Inversion by Res2Dinv

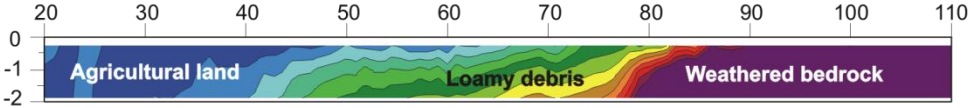

Measured Apparent Resistivity Pseudosection

Iteration 3 RMS error = 4.7 %

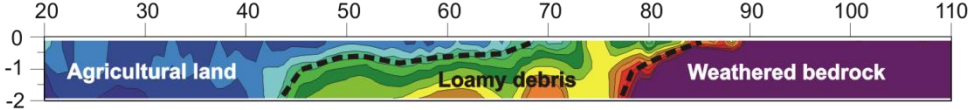

Inverse Model Resistivity Section

Resistivity in ohm.m

GF Instruments, s.r.o.
Geophysical Equipment and Services

Farming and Woodland Area
Resistivity Slices of Shallow Soil Structures

Measured with CMD-Mini Explorer

3D Imaging and Inversion by Res3Dinv

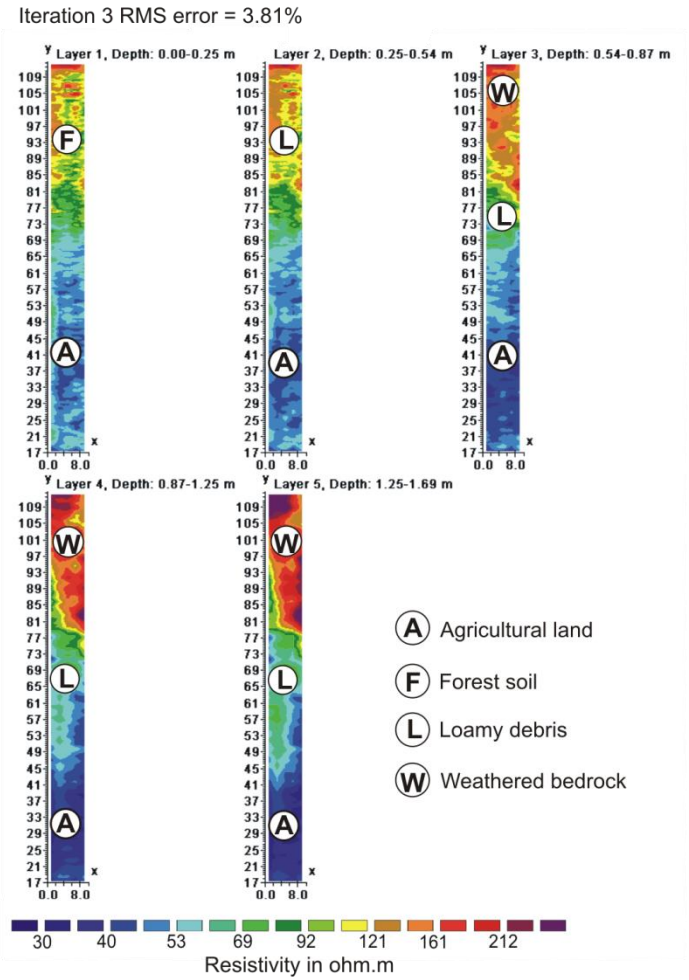

GF Instruments, s.r.o.
Geophysical Equipment and Services

Metal Pipeline Detection

Measurement was performed above metal pipeline. The goal of the measurement was to determine position and depth of the pipe.

The most effective ways of imaging are shown:

- Inphase maps from all three EM systems of CMD-MiniExplorer (with the biggest contrast at 1 m depth)
- Resistivity Section with 2D imaging and inversion by Res2Dinv (confirms 1 m depth of the pipe)

Metal Pipeline Detection
Contour Maps of Inphase

GF Instruments, s.r.o.
Geophysical Equipment and Services

Measured with CMD-Mini Explorer

Imaging by Surfer

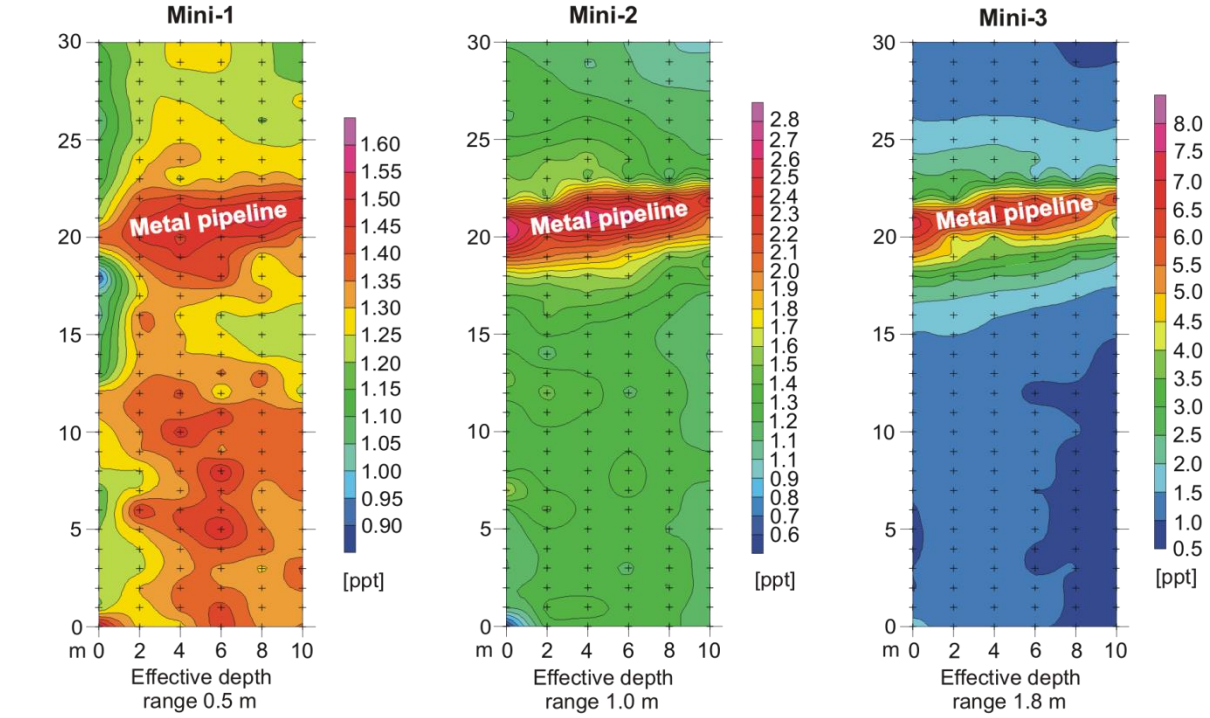

Metal Pipeline Detection
Resistivity Section

Measured with CMD-Mini Explorer

2D Imaging and Inversion by Res2Dinv

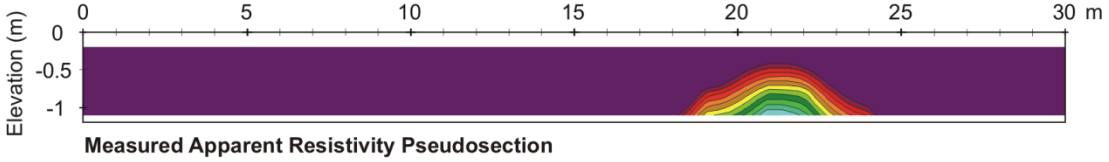

Measured Apparent Resistivity Pseudosection

Iteration 3 RMS error= 2.8 %

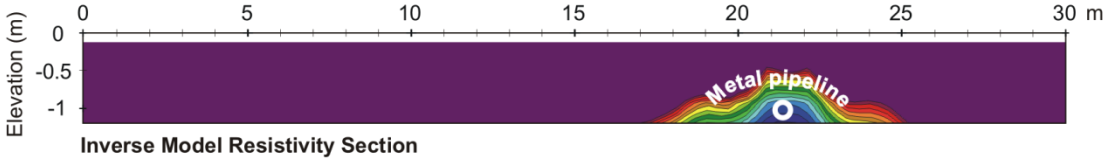

Inverse Model Resistivity Section

GF Instruments, s.r.o.
Geophysical Equipment and Services

Survey of the Settlement of the Bell Beaker Culture

Measurement was performed at the locality with surface archaeological findings to determine the area and depth of cultural layers.

Following pictures show:

- Six depth graded apparent resistivity maps made by CMD-MiniExplorer 6L
- Central inverse model resistivity section (measured with CMD-MiniExplorer 6L along line 20 with inversion by Res2Dinv) accompanied with reference inverse model resistivity section measured with ARES II with inversion by Res2Dinv (confirms the bottom line of cultural layers at the depth of about -1 m).

Survey of the Settlement of the Bell Beaker Culture
Apparent Resistivity Maps of Archaeological Site

GF Instruments, s.r.o.
Geophysical Equipment and Services

Measured with CMD-MiniExplorer 6L

Imaging by Surfer

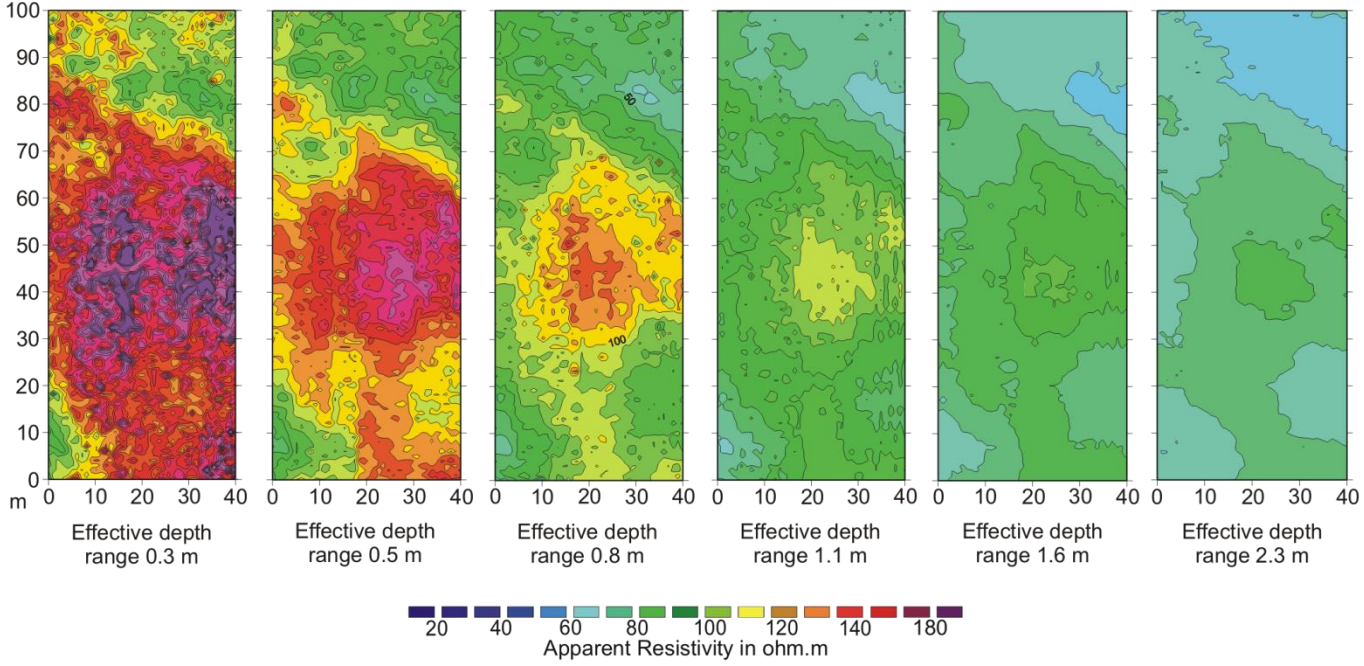

Survey of the Settlement of the Bell Beaker Culture
Central Inverse Model Resistivity Section

GF Instruments, s.r.o.
Geophysical Equipment and Services

Measured with CMD - MiniExplorer 6L

Inversion by Res2DInv (Iteration Abs. error = 4.4 ohm.m) and imaging by Surfer

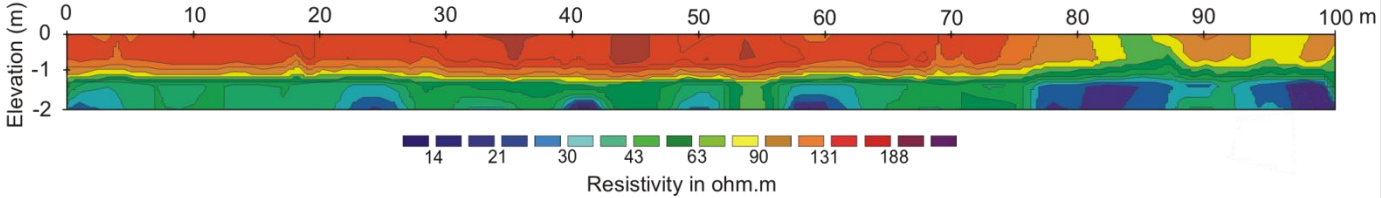

Reference Central Inverse Model Resistivity Section

Measured with ARES II using Schlumberger array (Unit electrode spacing 0.5m)

Inversion by Res2DInv (Iteration Abs. error = 2.5 ohm.m) and imaging by Surfer

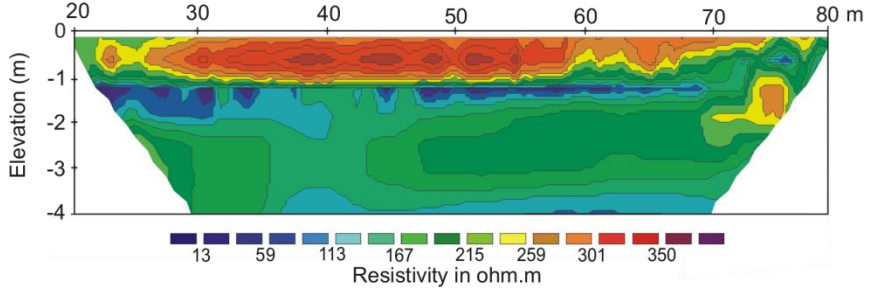

Chapter 3
Examples of typical applications

Engineering survey, road and railway building
- judgment of bedrock
- detection of cellars, cables, pipes
- assessment of mechanical properties of rocks

Dams and dikes (flood protection)
- localization of watered zones and landslides
- mapping of impacts
- beaver holes detection

Water management
- water source survey and protection
- monitoring of waste water leakage

Geological mapping
- raw material prospecting
- geological survey
- cavities detection

Agriculture
- soil quality monitoring
- fertilizer and watering management

Archaeology
- detection of remains of walls, cellars, vaults
- detailed survey of historical sites (graves, settlements)
- localization of underground corridors

Environmental

- mapping of pollution plumes
- survey of illegal waste dumps
- monitoring of leakages from agricultural and industrial plants

Military and police

- pioneer work
- UXO survey
- detection of graves and hidden objects

Comment:
Instruments CM-031, CM-032 and CM-138 are older versions of up-to-date CMD-4, CMD-2 and CMD-1 probes.

Engineering geology survey for road reconstruction

GF Instruments, s.r.o.
Geophysical Equipment and Services

Limestone cliff decay in marginal part of Moravian karst was endangering the road built over river sink and caves (falling blocks of walls and sediments were taken by sinking underground river).
The road reconstruction based on new bridge over destroyed part was considered.
The map shows places with solid limestone blocks, depresion filled with terra rosa and other instable structures.

Measured with electromagnetic conductivity meter CM-031

Contour map of apparent resistivity

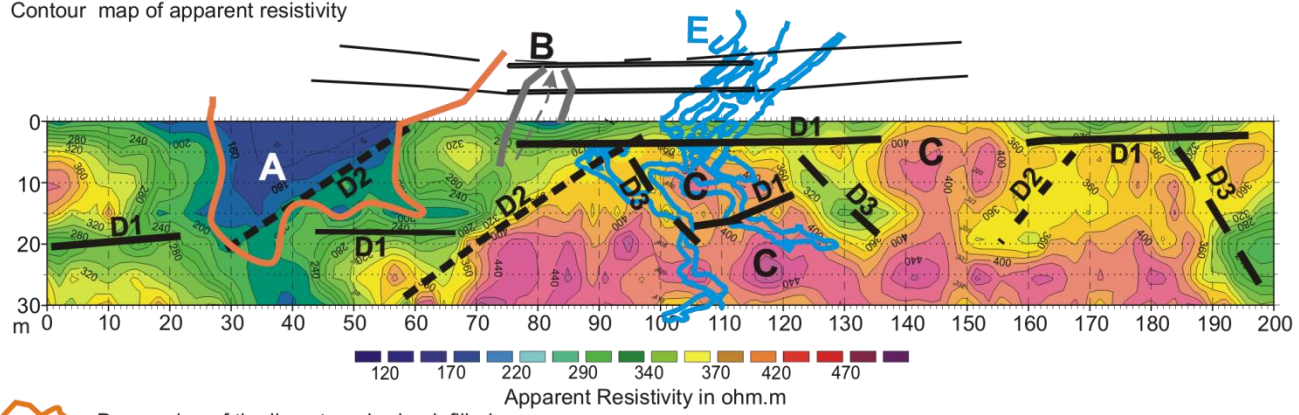

A Depression of the limestone bedrock filled with loams and sandy loams

Course of surface and groundwater

D1 Deformation parallel with slopes

D2 Direction of limestones

D3 Deformation parallel with tectonics

B Risk zone **C** Limestone crags **E** Geodeticaly fixed caves

Mapping slope deformation

A road was fatally destroyed by active landslide as a consequence of heavy rain. Detailed monitoring of the slope was performed before road reconstruction to detect instable zones.

The position of extremely risky watered zone is seen on the picture. Water accumulation below the road (damaged dewatering system) and consequent permanently watered sediments activate continuous landslide. The probable directions of outflow show the possibility of activation of the mass of old landslides.

Measured with electromagnetic conductivity meter CM-031

Contour map of apparent resistivity

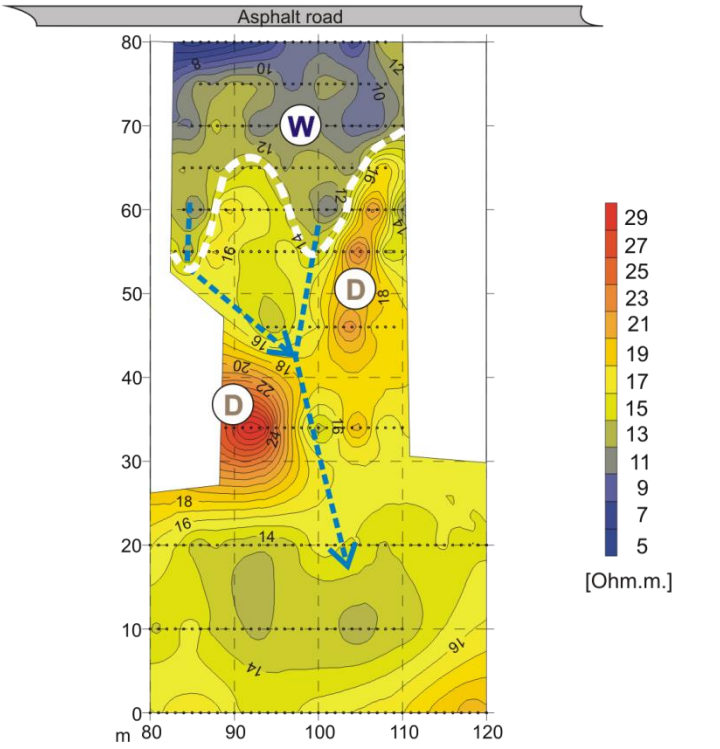

Monitoring of road body

GF Instruments, s.r.o.
Geophysical Equipment and Services

This survey shows the possibility of fast monitoring of road body quality accompanied with information about geological structure of bedrock.
Two maps were obtained using probes with different depth ranges. The first map (CM-032) shows irregular structure of construction materials - sand and gravel (high resistive) with different width and thickness. The second map (CM-031) shows rather homogenous clayey bedrock.

Measured with electromagnetic conductivity meter CM-032

Contour map of apparent resistivity

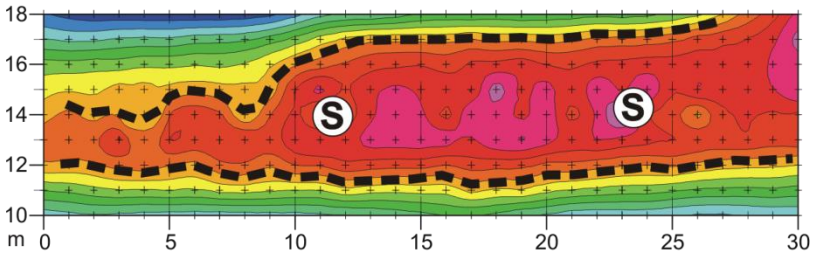

Measured with electromagnetic conductivity meter CM-031

Contour map of apparent resistivity

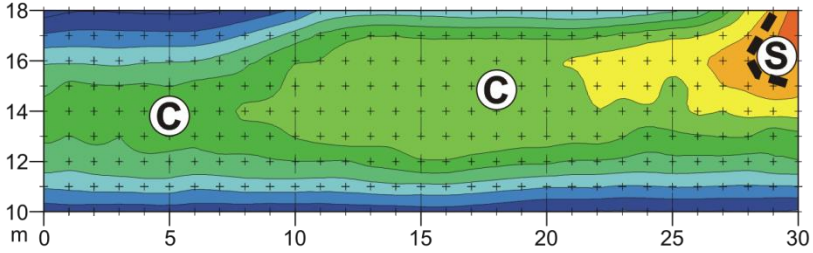

C Clay loam

S Sand and gravel

Mapping road stability

Continuing road destruction was studied using two measurements with different depth ranges.
Obtained maps show that the clayey zone (as the main reason of landslide) is situated rather in deeper part of road basement. Both maps show increased moisture below the damaged place. Its measure increases with the depth.

Measured with electromagnetic conductivity meter CM-032

Contour map of apparent resistivity

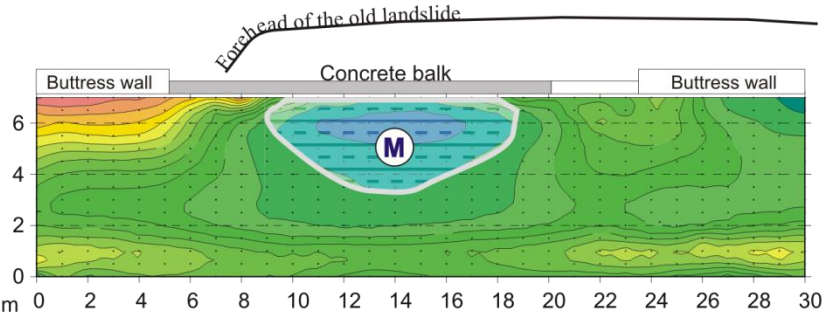

Measured with electromagnetic conductivity meter CM-031

Contour map of apparent resistivity

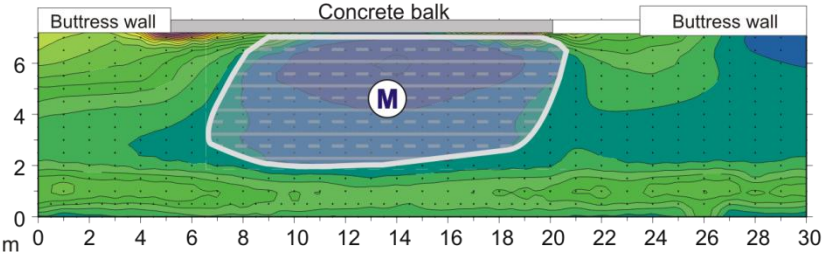

M Area with increased moisture and caverns filled with clayey mud

GF Instruments, s.r.o.
Geophysical Equipment and Services

Buried metal pipeline detection

The metal pipeline was detected at about 1 m depth. Its position is indicated with very strong and narrow anomaly - increased values of inphase.

Measured with electromagnetic conductivity meter CMD 2

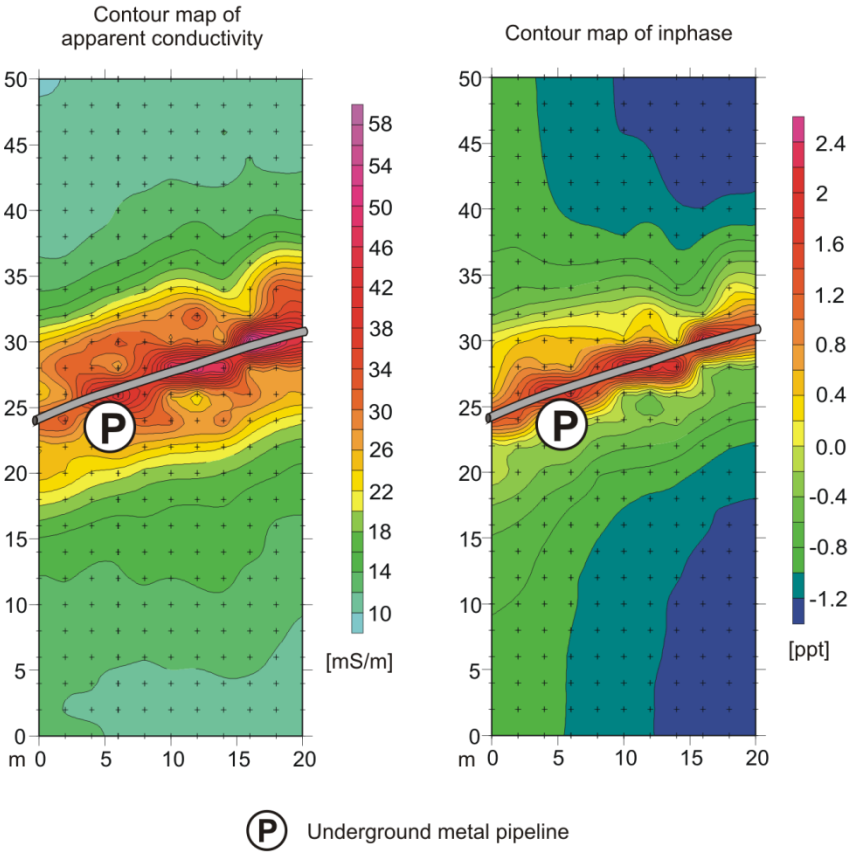

Mapping underground objects

GF Instruments, s.r.o.
Geophysical Equipment and Services

Area of former starch factory was investigated to determine positions of pipelines and other buried objects before projecting of new commercial centre.

The map shows inhomogeneous structure of backfill in former potato yard (random direct investigation discovered building waste material, concrete blocks and other waste material). The position of basement of industrial track and two pipelines are visible as well.

Measured with electromagnetic conductivity meter CM-032

Contour map of apparent resistivity

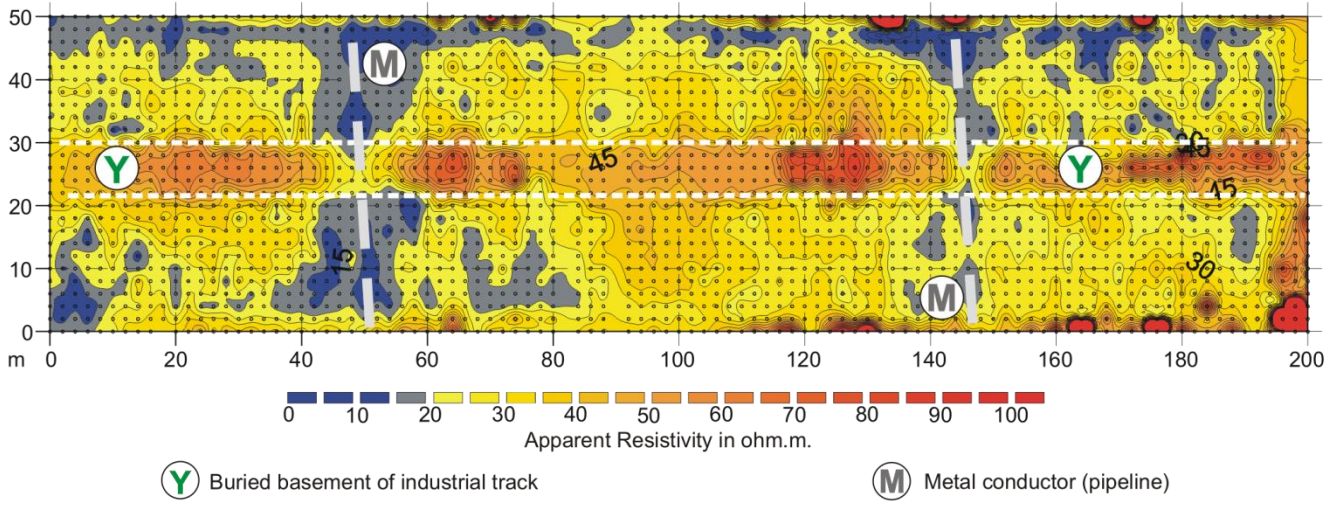

Dike investigation

Searching for cavities in the fishpond dike. The fishpond dike was partially destroyed during the flood. The survey was performed to detect its weak places.

The low resistivity indicates larger destructed zones (voids) filled with water and mud.

Measured with electromagnetic conductivity meter CM-032

Contour map of apparent resistivity

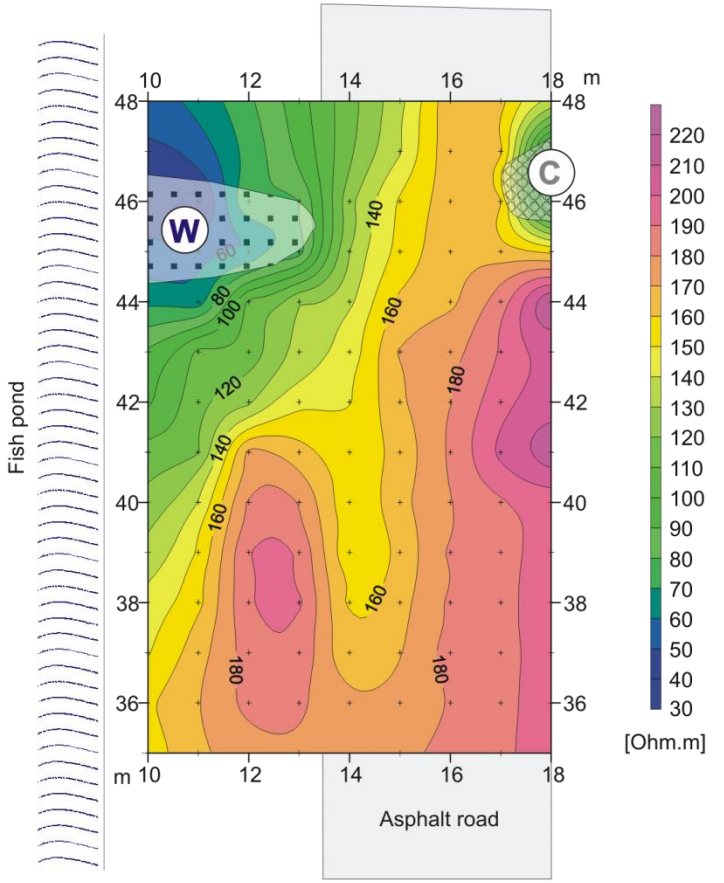

W Cave filled with water

C Cave repaired with concrete grouting

GF Instruments, s.r.o.
Geophysical Equipment and Services

Determination of the penetration of sodium sulphate from a mud pit

The mud pit is filled during the mining technology process wih the solution containing sodium sulphate. The conductivity measurement was done to monitor the tightness of the dam and the efficiency of the dewatering ditches along the dam. One part of the long area under the dam was chosen for the survey.

The measure of the contamination is obvious from the apparent conductivity map. The measure of underground water pollution with sodium sulphate decreases homogenously with the distance from the dewatering ditch.

The inphase map copies the conductivity map on the great part of the measured area showing that no burried metallic objects are present. The bottom part of the inphase map is influenced by the dewatering ditch and the concrete pavement reinforcement.

Measured with electromagnetic conductivity meter CM-031

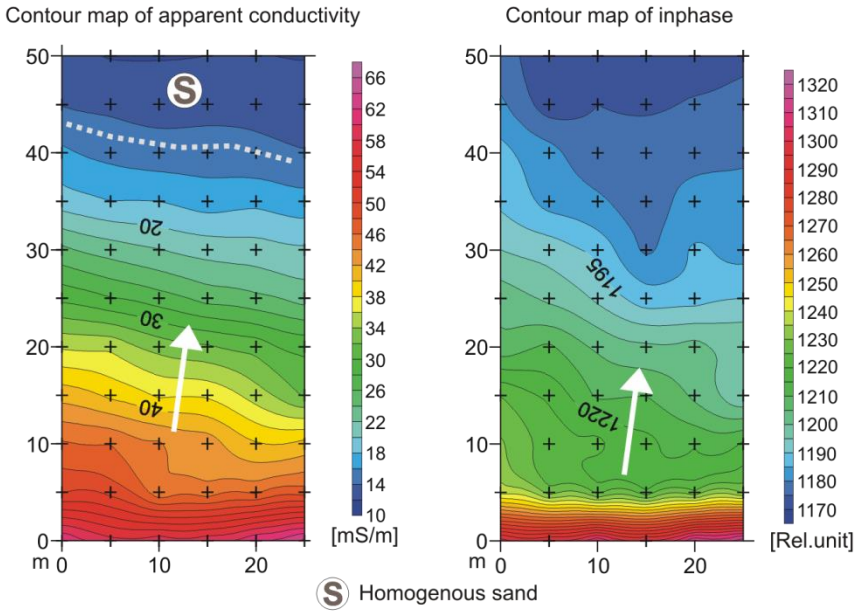

Geological mapping

Geological mapping before construction of new highway crossing was performed. The recent agriculture area (on former gravel deposit) was investigated before digging of the basement of the road overpass.

The map shows precisely the position of exploited gravel deposit filled with inhomogeneous rubbish. This area is typical with low resistivity (remains of organic mass).

Measured with electromagnetic conductivity meter CM-031

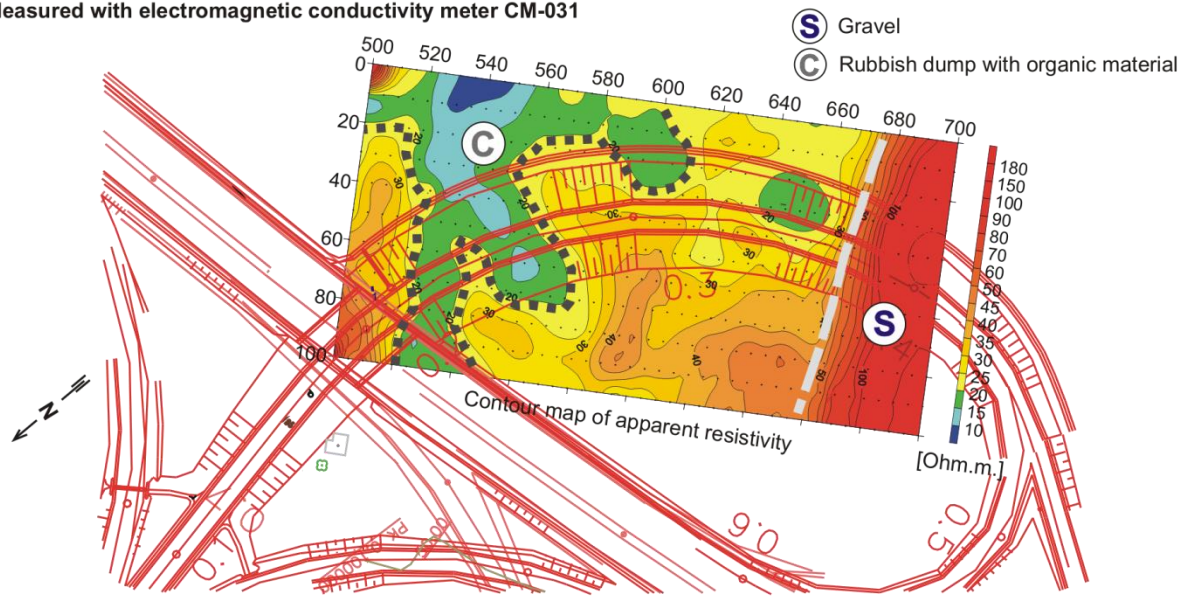

Archaeology

Detailed mapping of foundations of abolished Sanctus Vitus chapel from 1263 had to verify roman vault situated on the former cemetery.

Two maps from various depths allow distinguishing individual parts and shape of the chapel.
The CM-138 map shows rather detailed structure near surface while the position of the vault as well as shape of basements and position of peripheral walls are seen in CM-031 map.

Measured with electromagnetic conductivity meter CM-031

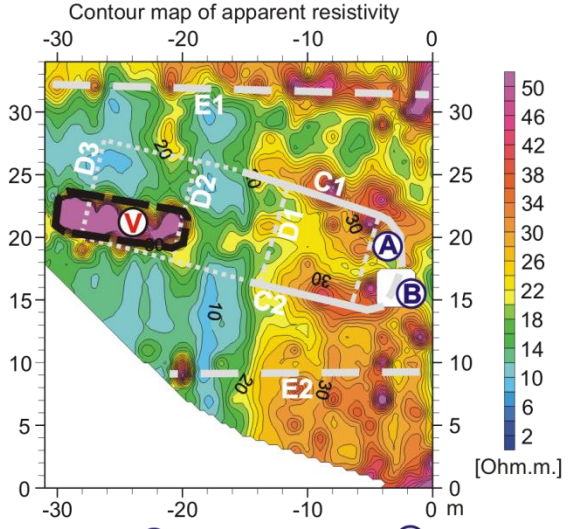

Measured with electromagnetic conductivity meter CM-138

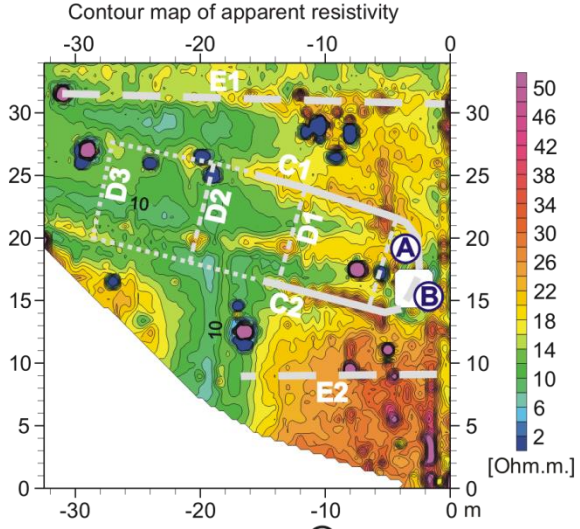

Ⓐ Presbiterium
Ⓑ Metallic enclosure with metallic cross inside
Ⓥ Old vault
C1, C2 Main foundation lines
D1, D2, D3 Cross foundation lines
E1, E2 Indications of the peripheral walls

Archaeology

Identification of hidden parts of fortification was performed to complete formerly discovered walls and underground objects of medieval castle.

The map with two high resistive stone objects corresponds with remains of a gate (or pillars). The left part of the picture shows the area of outer court.

Measured with electromagnetic conductivity meter CM-031

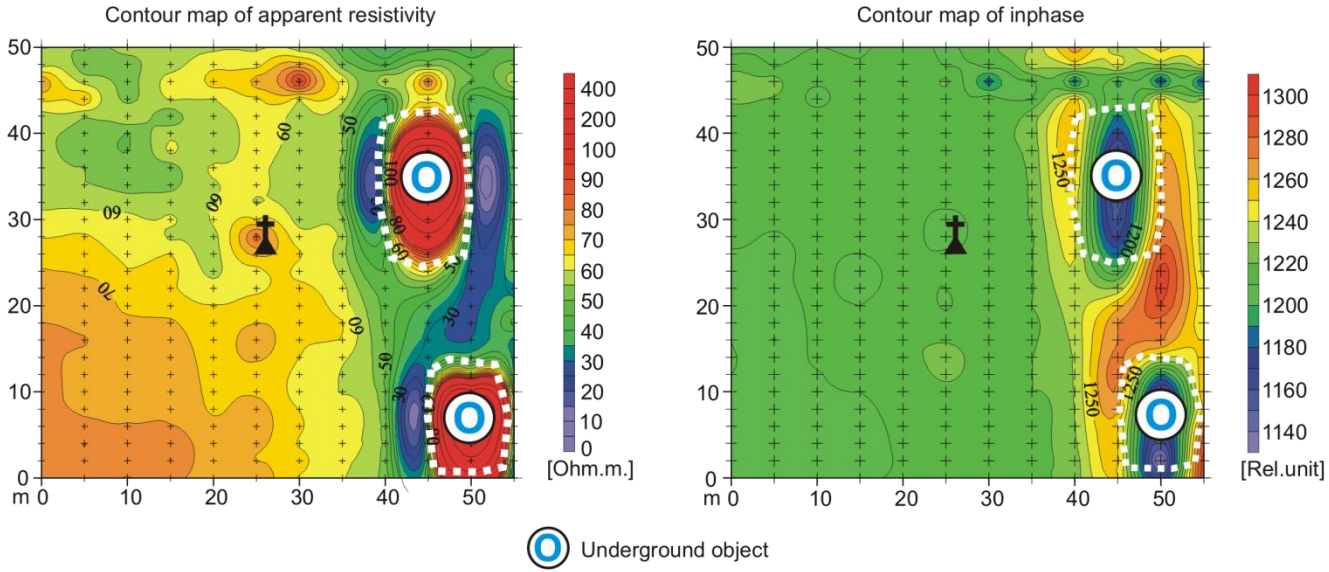

GF Instruments, s.r.o.
Geophysical Equipment and Services

Environmental protection

The studied area was inside a uranium mining field. During the mining process a technologic difficulty occured and the sulphuric acid leaked out from a plastic pipe near to one of boreholes. The determination of the pollution plume was needed to allow sanation works in the area.

The direction and the measure of the propagation of the acid flow are indicated with higher values of apparent conductivity.

Measured with electromagnetic conductivity meter CM-031

Contour map of apparent conductivity

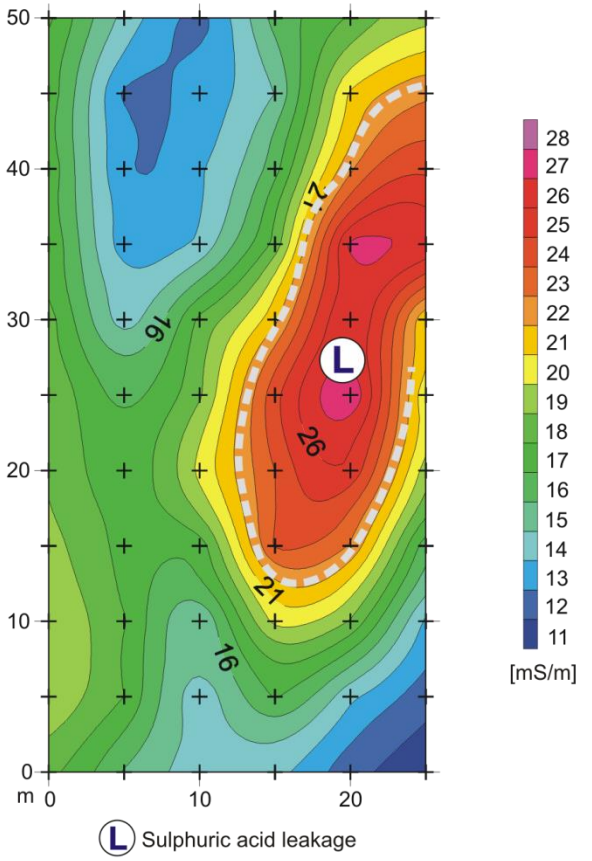

GF Instruments, s.r.o.
Geophysical Equipment and Services

Environmental protection

A complex monitoring in the frame of ground water protection in close vicinity of a pig farm was done. The goal was to detect leakage from a liquid manure tank.
The decreased resistivity indicates the zone with contamination. These extremely low values of resistivity are typical for the high contamination with organic substances.

Measured with electromagnetic conductivity meter CM-031

Contour map of apparent resistivity

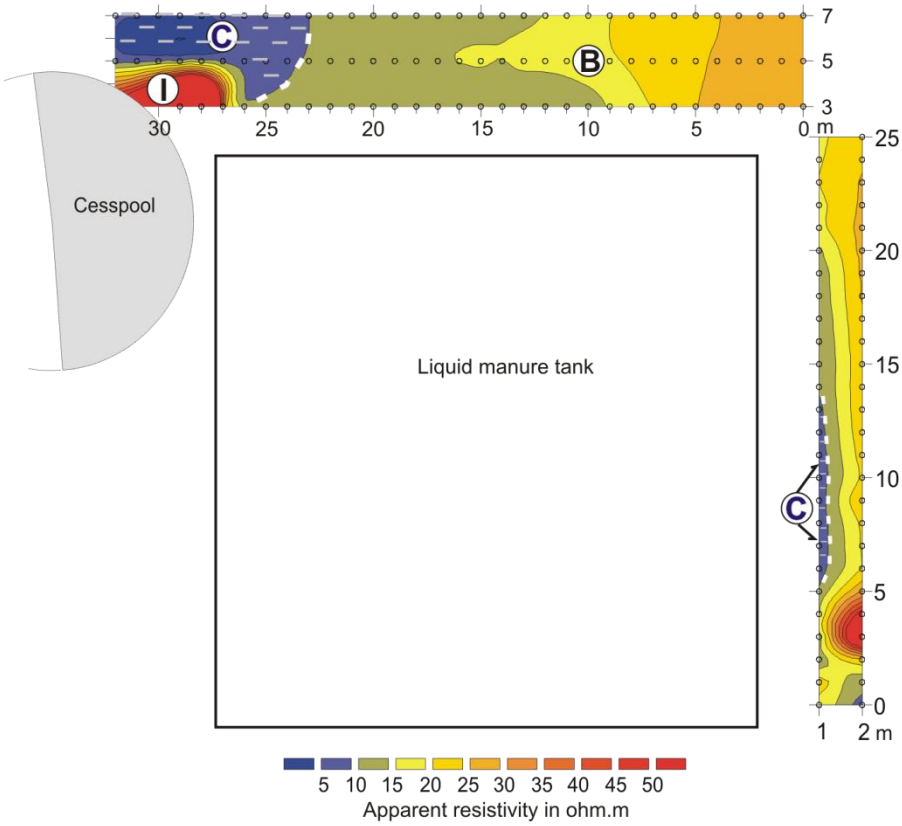

B Backfill - sand and gravel

C Zone of contamination with liquid manure

I Influence of reinforced concrete centring

GF Instruments, s.r.o.
Geophysical Equipment and Services

Mapping of buried waste dump

Higher values of conductivity indicate the area formed with homogenous clay sediments. High variability and low values of conductivity are typical for the inhomogeneous landfill (without organic material). The inphase map shows a lot of metallic objects in landfill (increased inphase).

Measured with electromagnetic conductivity meter CMD 4

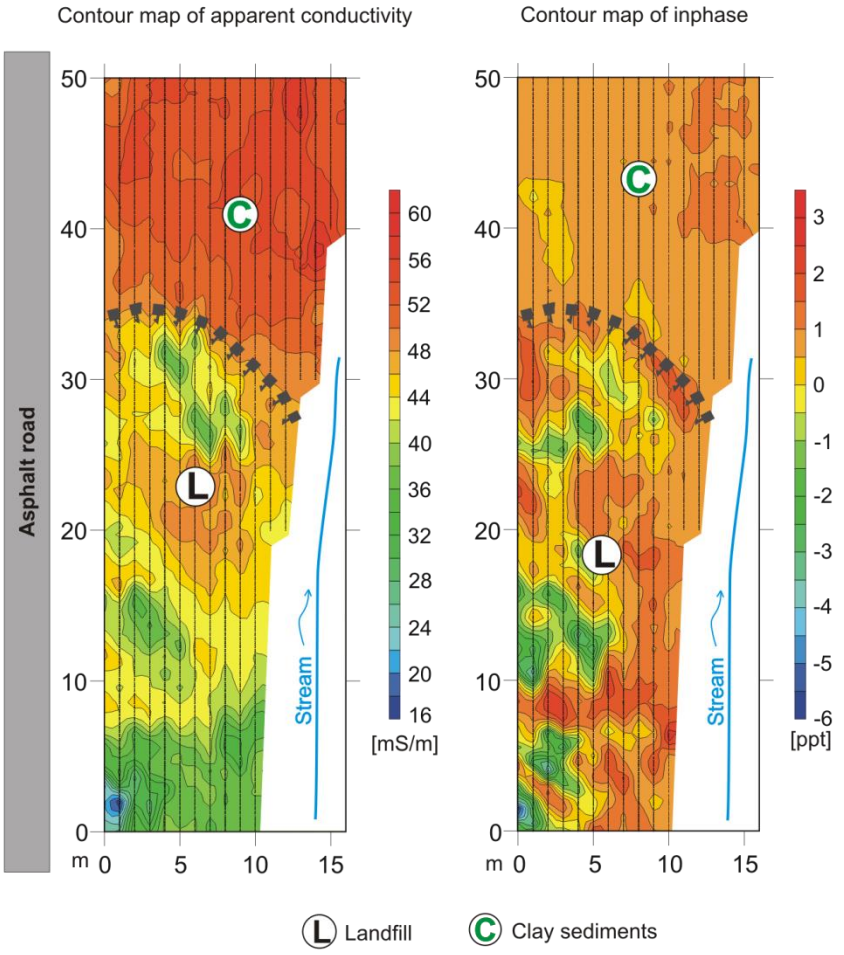

Detection of buried objects

GF Instruments, s.r.o.
Geophysical Equipment and Services

Geophysical survey was performed to detect underground objects from World War II. Several objects were identified. There are two concrete bunkers connected with trenches serving for treatment of city inhabitants and workers from close factory. The central low resistive bended zone shows former watershed filled with conductive sediments.

Measured with electromagnetic conductivity meter CM-031

Contour map of apparent resistivity

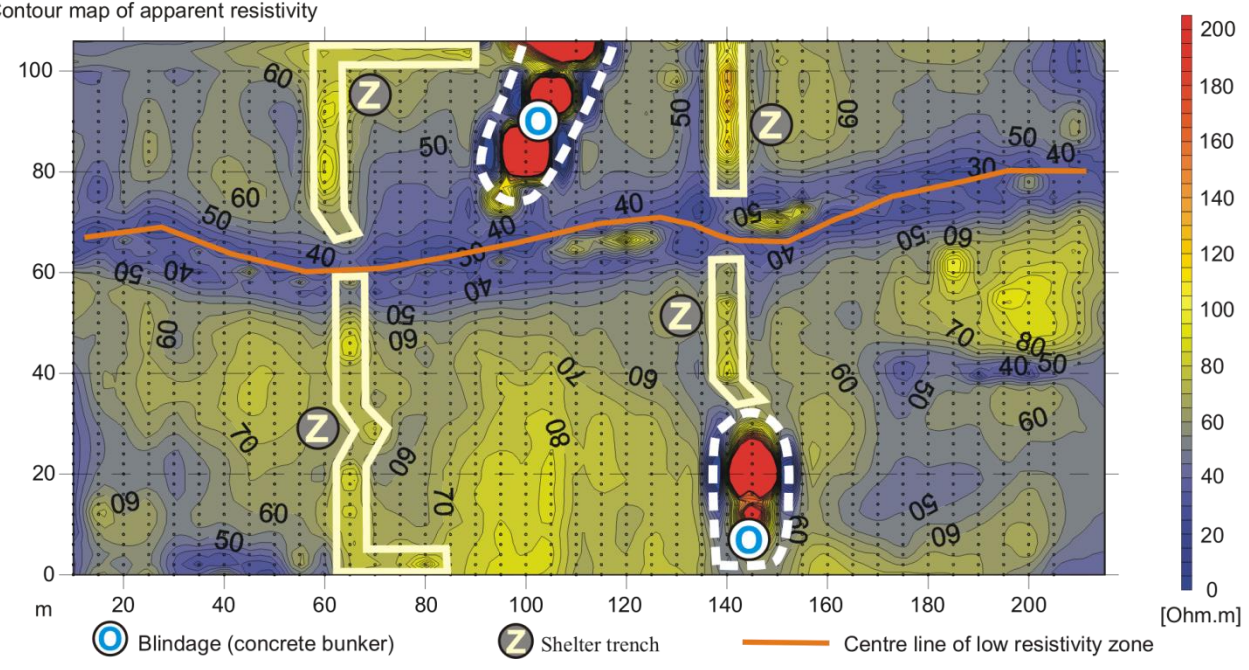

Physical Theory of Electromagnetic Conductivity Measurement Low Induction Number Approximation

by Hana Růžičková

This chapter brings a complex mathematical derivation based on Maxwell equations of electromagnetic field. Our intention is to describe both all important mathematical crossings together with physical simplifications and their final impacts on measuring features of electromagnetic conductivity meters. Such complex analysis is not usual for electromagnetic geophysical literature (e.g. G. V. Keller, S. Mareš). The analysis is completed with derivation of formulae for calculation of depth-depending normalized sensitivity of antennas.
The coplanar (slingram) configuration of transmitter and receiver coils is analysed in vertical and horizontal positions. Individual mathematical and physical steps are commented as they follow. Some used procedures come from the article by S. H. Ward and G. W. Hohmann (1988).

We assume all material constants are only frequency-dependent; we work with non-magnetic environment.

$$\vec{D} = \varepsilon\vec{E},\ \vec{j} = \sigma\vec{E},\ \vec{B} = \mu\vec{H},\ \mu = \mu_0,$$

where $\vec{D}$ is electric displacement field, $\vec{E}$ is electric field intensity, $\vec{B}$ is magnetic field, $\vec{H}$ is magnetic field, $\vec{j}$ is current density, ε is permittivity, σ is conductivity and μ is permeability with μ_0 for vacuum. We use harmonic current, i.e. $I \sim \mathrm{e}^{\mathrm{i}\omega t}$, where I is current, ω is angular frequency and t is time. Therefore both $\vec{E}$ and $\vec{H} \sim \mathrm{e}^{\mathrm{i}\omega t}$, $\frac{\partial\vec{H}}{\partial t} = \mathrm{i}\omega\vec{H}$ and $\frac{\partial\vec{E}}{\partial t} = \mathrm{i}\omega\vec{E}$.
Maxwell equations in homogeneous medium:

$$\nabla \times \vec{H} = \vec{j} + \frac{\partial\vec{D}}{\partial t} = \sigma\vec{E} + \varepsilon\frac{\partial\vec{E}}{\partial t} = (\sigma + \mathrm{i}\omega\varepsilon)\,\vec{E} \tag{1}$$

$$\nabla \times \vec{E} = -\frac{\partial\vec{B}}{\partial t} = -\mu_0\frac{\partial\vec{H}}{\partial t} = -\mathrm{i}\omega\mu_0\vec{H}$$

$$\nabla\vec{D} = \varepsilon\nabla\vec{E} = 0$$

$$\nabla\vec{B} = \mu_0\nabla\vec{H} = 0$$

For space with field sources we need to have inhomogeneous equations. We assume only magnetic inhomogeneities.

$$\nabla \times \vec{E} + \mathrm{i}\omega\mu_0\vec{H} = -\vec{J}_{\mathrm{mag}} \tag{2}$$

For further mathematical purposes we define $\vec{F}$:

$$\vec{E} = -\nabla \times \vec{F}$$

From (1) we get $\vec{H} = -(\sigma + \mathrm{i}\omega\varepsilon)\vec{F} - \nabla U$, where U is an arbitrary scalar with useful calibration $\nabla\vec{F} = -\mathrm{i}\omega\mu_0 U$. Inserting all this into (2), we obtain

$$\nabla^2\vec{F} + k_0^2\vec{F} = -\vec{J}_{\mathrm{mag}},$$

where $k_n^2 = \mu_0\varepsilon_n\omega^2 - \mathrm{i}\omega\sigma_n\mu_0$ and $n = 0$ denotes air. We work with low frequencies, so $\mu_0\varepsilon_n\omega^2 \ll \omega\sigma_n\mu_0$ and $k_n = \sqrt{-\mathrm{i}\omega\mu_0\sigma_n}$. As we can assume all our sources to be magnetic dipoles (current loops from far enough), it is sufficient for $\vec{F}$ to have only one component in the dipole direction. Therefore it is enough now to solve only one scalar equation.

Vertical magnetic dipole

We assume a vertical magnetic dipole in the z-direction above earth with $z = 0$ boundary, m is magnetic moment of the dipole.

$$\nabla^2 F + k_0^2 F = -\mathrm{i}\omega\mu_0 m\delta(x)\delta(y)\delta(z)$$

For easier mathematical processing we introduce 3D Fourier transform and apply it to the equation above:

$$F^{3\mathrm{DF}}(k_x, k_y, k_z) = \int_{-\infty}^{\infty}\int_{-\infty}^{\infty}\int_{-\infty}^{\infty} F(x,y,z)\mathrm{e}^{-\mathrm{i}(k_x x + k_y y + k_z z)}\,\mathrm{d}x\mathrm{d}y\mathrm{d}z$$

$$(-k_x^2 - k_y^2 - k_z^2 + k_0^2)F^{3\mathrm{DF}} = (-\mathrm{i}\omega\mu_0 m\delta(x)\delta(y)\delta(z))^{3\mathrm{DF}}$$

$$F^{3\mathrm{DF}} = \frac{\mathrm{i}\omega\mu_0 m}{k_x^2 + k_y^2 + k_z^2 - k_0^2}$$

We integrate over k_z (earth is perpendicular to z):

$$F^{2\mathrm{DF}}(k_x, k_y, z) = \frac{\mathrm{i}\omega\mu_0 m}{2\pi}\int_{-\infty}^{\infty}\frac{\mathrm{e}^{\mathrm{i}k_z z}}{k_x^2 + k_y^2 + k_z^2 - k_0^2}\,\mathrm{d}k_z = \frac{\mathrm{i}\omega\mu_0 m\mathrm{e}^{-u_0|z|}}{2u_0},$$

where $u_n = \sqrt{k_x^2 + k_y^2 - k_n^2}$. Knowing the z-dependence we assume our solution to be

$$F^{2\mathrm{DF}}(k_x, k_y, z) = \frac{\mathrm{i}\omega\mu_0 m}{2u_0}\left(\mathrm{e}^{-u_0 z} + r\mathrm{e}^{u_0 z}\right),$$

where the first term contains the amplitude of the incident electromagnetic wave going from the source to the boundary and the second term is the refracted wave with r being the amplitude reflection coefficient of normal incidence (from Fresnel conditions) $r = \frac{u_0 - u_1}{u_0 + u_1}$. Indices 0 refer to the air, 1s are for earth. We perform inverse 2D Fourier transform (only two integrals remain):

$$F(x,y,z) = \frac{\mathrm{i}\omega\mu_0 m}{8\pi^2} \int_{-\infty}^{\infty}\int_{-\infty}^{\infty} \left(\mathrm{e}^{-u_0 z} + r\mathrm{e}^{u_0 z}\right) \frac{1}{u_0} \mathrm{e}^{\mathrm{i}(k_x x + k_y y)}\,\mathrm{d}k_x \mathrm{d}k_y$$

For rotationally symmetric functions we can convert to a Hankel transform:

$$F(\rho,z) = \frac{\mathrm{i}\omega\mu_0 m}{4\pi} \int_0^{\infty} \left(\mathrm{e}^{-u_0 z} + r\mathrm{e}^{u_0 z}\right) \frac{\lambda}{u_0} \mathrm{J}_0(\lambda\rho)\,\mathrm{d}\lambda, \tag{3}$$

where $\lambda^2 = k_x^2 + k_y^2$, $\rho^2 = x^2 + y^2$ and $\mathrm{J}_0(x)$ is a Bessel function. Electric field has only angular component $E_\varphi = -\frac{y}{\rho}E_x + \frac{x}{\rho}E_y$. Using identities

$$\frac{\partial \mathrm{J}_0(\lambda\rho)}{\partial x} = -\lambda\frac{x}{\rho}\mathrm{J}_1(\lambda\rho),\ E_x = -\frac{\partial F}{\partial y},\ E_y = \frac{\partial F}{\partial x}$$

$$E_\varphi = -\frac{\mathrm{i}\omega\mu_0 m}{4\pi} \int_0^{\infty} \left(\mathrm{e}^{-u_0 z} + r\mathrm{e}^{u_0 z}\right) \frac{\lambda^2}{u_0} \mathrm{J}_1(\lambda\rho)\,\mathrm{d}\lambda$$

We assume dipoles to be in non-conductive air: $k_0 = 0$, $u_0 = \lambda$. Then $k_1 = k = \sqrt{-\mathrm{i}\omega\mu_0\sigma}$ and $u_1 = u$. We are looking for solution in $z = 0$ (both transmitter and receiver are on the ground):

$$\begin{aligned} E_\varphi &= -\frac{\mathrm{i}\omega\mu_0 m}{2\pi} \int_0^{\infty} \frac{\lambda^2}{\lambda + u} \mathrm{J}_1(\lambda\rho)\,\mathrm{d}\lambda = \frac{\mathrm{i}\omega\mu_0 m}{2\pi} \frac{\partial}{\partial\rho} \int_0^{\infty} \frac{\lambda}{\lambda + u} \mathrm{J}_0(\lambda\rho)\,\mathrm{d}\lambda \\ &= \frac{\mathrm{i}\omega\mu_0 m}{2\pi k^2} \frac{\partial}{\partial\rho} \left[\int_0^{\infty} \lambda^2 \mathrm{J}_0(\lambda\rho)\,\mathrm{d}\lambda - \int_0^{\infty} \lambda u \mathrm{J}_0(\lambda\rho)\,\mathrm{d}\lambda\right] \end{aligned}$$

Identities:

$$\int_0^{\infty} \mathrm{e}^{-\lambda z} \mathrm{J}_0(\lambda\rho)\,\mathrm{d}\lambda = \frac{1}{\sqrt{\rho^2 + z^2}} \tag{4}$$

$$\int_0^{\infty} \frac{\lambda}{u} \mathrm{e}^{-uz} \mathrm{J}_0(\lambda\rho)\,\mathrm{d}\lambda = \frac{\mathrm{e}^{-\mathrm{i}k\sqrt{\rho^2+z^2}}}{\sqrt{\rho^2 + z^2}}$$

$$\begin{aligned} E_\varphi &= -\frac{m}{2\pi\sigma} \frac{\partial}{\partial\rho} \left[\frac{\partial^2}{\partial z^2} \frac{1}{\sqrt{\rho^2 + z^2}} - \frac{\partial^2}{\partial z^2} \frac{\mathrm{e}^{-\mathrm{i}k\sqrt{\rho^2+z^2}}}{\sqrt{\rho^2 + z^2}}\right]_{z=0} \\ &= -\frac{m}{2\pi\sigma\rho^4} \left[3 - \left(3 + 3\mathrm{i}k\rho - k^2\rho^2\right) \mathrm{e}^{-\mathrm{i}k\rho}\right] \end{aligned}$$

Maxwell equation in cylindrical coordinates:

$$H_z = -\frac{1}{\mathrm{i}\omega\mu_0}\frac{1}{\rho}\frac{\partial}{\partial\rho}(\rho E_\varphi)$$

Secondary magnetic field in z-direction:

$$H_z^s = \frac{m}{2\pi k^2\rho^5}\left[9-\left(9+9\mathrm{i}k\rho-4k^2\rho^2-\mathrm{i}k^3\rho^3\right)\mathrm{e}^{-\mathrm{i}k\rho}\right],$$

with ρ being the distance between the coil centers. Primary field (magnetic dipole in free space):

$$\vec{H}(\vec{r}) = \frac{1}{4\pi r^3}\left[3(\vec{m}\vec{r})\vec{r}-\vec{m}\right]$$

$$H_z^p = -\frac{m}{4\pi\rho^3}$$

For $\gamma = \mathrm{i}k$ we get frequently published McNeill's equation

$$\frac{H^s}{H^p} = \frac{2}{\gamma^2\rho^2}\left[9-\left(9+9\gamma\rho+4\gamma^2\rho^2+\gamma^3\rho^3\right)\mathrm{e}^{-\gamma\rho}\right] \tag{5}$$

We introduce the induction number: $B = \frac{\gamma\rho}{\sqrt{2\mathrm{i}}}$.

$$\frac{H^s}{H^p} = -\frac{9\mathrm{i}}{B^2}\left[1-\left(1+B+\mathrm{i}B+\frac{8}{9}\mathrm{i}B^2-\frac{2}{9}B^3+\frac{2}{9}\mathrm{i}B^3\right)\mathrm{e}^{-B}\mathrm{e}^{-\mathrm{i}B}\right]$$

We are interested in the quadrature, i.e. imaginary part:

$$\left(\frac{H^s}{H^p}\right)_{\mathrm{q}} = \frac{-9\mathrm{i}}{B^2}\left[1-\left(B+\frac{8}{9}B^2+\frac{2}{9}B^3\right)\mathrm{e}^{-B}\sin B-\left(1+B-\frac{2}{9}B^3\right)\mathrm{e}^{-B}\cos B\right]$$

Taylor expansion for small B:

$$\left(\frac{H^s}{H^p}\right)_{\mathrm{q}} = \mathrm{i}\left[\frac{B^2}{2}-\frac{8B^3}{15}+\frac{16B^5}{105}-\frac{5B^6}{72}+\mathcal{O}(B^7)\right] \tag{6}$$

For very small B:

$$\left(\frac{H^s}{H^p}\right)_{\mathrm{q}}^{\mathrm{V}} \approx \frac{\mathrm{i}B^2}{2} = \frac{\gamma^2\rho^2}{4} = \frac{\mathrm{i}\sigma\mu_0\omega\rho^2}{4}$$

This formula is typical for the linear part of the calibration curve of electromagnetic conductivity meters. With increasing induction number the second term of the expansion (6) gives a distinct negative contribution, which results in the decreasing part of the calibration curve and ambiguous results of measurements.
Now we can express the apparent conductivity σ^{V}:

$$\sigma^{\mathrm{V}} = \frac{4}{\mathrm{i}\mu_0\omega\rho^2}\left(\frac{H^s}{H^p}\right)^{\mathrm{V}}_{\mathrm{q}} \tag{7}$$

When we look at the real part of (5), we get

$$\Re\left(\frac{H^s}{H^p}\right) = \frac{9}{B^2}\left[\left(1+B-\frac{2}{9}B^3\right)\mathrm{e}^{-B}\sin B - \left(B+\frac{8}{9}B^2+\frac{2}{9}B^3\right)\mathrm{e}^{-B}\cos B\right]$$

Taylor expansion for small B:

$$\Re\left(\frac{H^s}{H^p}\right) = 1+\frac{8B^3}{15}-\frac{B^4}{2}+\frac{16B^5}{105}+\mathcal{O}(B^6)$$

For very small B:

$$\Re\left(\frac{H^s}{H^p}\right)^{\mathrm{V}} = 1+\frac{4\sqrt{2}}{15}\left(\omega\mu_0\sigma\right)^{\frac{3}{2}}\rho^3$$

From this formula we can see that after subtraction of the primary field (number one – the first term) the most significant term contains a contribution of ground conductivity. This is undesirable effect for using in-phase to measure magnetic susceptibility.

Vertical dipole – depth-depending sensitivity

In the last chapter we considered earth to be a homogeneous medium with measurable apparent conductivity. Now we assume layered earth. We will continue from equation (3), but this time instead of inserting reflection coefficient of homogeneous halfspace in it, we will derive an expression for cumulative reflection from an infinite number of layers according to Optics of Thin Films by Z. Knittl.
From Fresnel conditions at normal incidence we get for one boundary between materials 0 and 1 these reflection and transmission coefficients:

$$r_{0\to1} = \frac{u_0-u_1}{u_0+u_1},\ r_{1\to0} = \frac{u_1-u_0}{u_0+u_1} \tag{8}$$

$$t_{0\to1} = \frac{2u_0}{u_0+u_1},\ t_{1\to0} = \frac{2u_1}{u_0+u_1}, \tag{9}$$

where $u_n = \sqrt{\lambda^2 - k_n^2}$ as before. Let us consider a reflection coefficient of two boundaries separated by a distance d. Initial electromagnetic wave can either reflect back (first term in the following expression) or pass through the first boundary. This part of the wave partly reflects back by the second boundary and then either passes through the first one (the second term) or reflects again towards the second boundary where the process repeats with decreasing amplitude.

$$\begin{aligned} r_{2\mathrm{b}} &= r_{0\to1} + t_{0\to1}r_{1\to2}t_{1\to0}\mathrm{e}^{-2du_1}\left(1+q+q^2+...\right) \\ q &= r_{1\to0}r_{1\to2}\mathrm{e}^{-2du_1} \end{aligned}$$

Summing the geometric progression and inserting from (8) and (9) we get

$$r_{2\mathrm{b}} = \frac{r_{0\to1} + r_{1\to2}\mathrm{e}^{-2du_1}}{1 + r_{0\to1}r_{1\to2}\mathrm{e}^{-2du_1}} \tag{10}$$

Now let us have a system of three boundaries separated into one simple boundary and a two-boundaries subsystem. Since we are interested only in the reflection, the subsystem behaves as a single boundary with reflection coefficient described in (10) and we get the same result for $r_{3\mathrm{b}}$ as above; only with $r_{2\mathrm{b}}$ instead of $r_{1\to2}$. Gradual adding of boundaries leads us to a recursive formula for a multilayer

$$r_j = \frac{r_{j\to j+1} + r_{j+1}\mathrm{e}^{-2d_{j+1}u_{j+1}}}{1 + r_{j\to j+1}r_{j+1}\mathrm{e}^{-2d_{j+1}u_{j+1}}},$$

where d_j is a distance between the j-th and $(j+1)$-st boundary (j-th layer). We use the low induction number approximation, so we have to perform a Taylor expansion of r_j around $\omega\mu_0\sigma_j \ll 1$ for every j, where σ_j is conductivity of the j-th layer:

$$r_j = \frac{\mathrm{i}\omega\mu_0\left(\sigma_j - \sigma_{j+1}\right)}{4\lambda^2} + r_{j+1}\mathrm{e}^{-2\lambda d_{j+1}} \tag{11}$$

To get the secondary magnetic field of vertical dipole we start from equation (3):

$$F(\rho,z) = \frac{\mathrm{i}\omega\mu_0 m}{4\pi}\int_0^\infty \left(\mathrm{e}^{-u_0 z} + r\mathrm{e}^{u_0 z}\right)\frac{\lambda}{u_0}\mathrm{J}_0(\lambda\rho)\,\mathrm{d}\lambda$$

$$H_z = \frac{1}{\mathrm{i}\omega\mu_0}\left(\frac{\partial^2}{\partial z^2} + k_0^2\right) F$$
$$= \frac{m}{4\pi}\int_0^\infty \left(\mathrm{e}^{-u_0 z} + r\mathrm{e}^{u_0 z}\right)\frac{\lambda^3}{\mu_0}\mathrm{J}_0(\lambda\rho)\,\mathrm{d}\lambda$$

Receiver is on the ground, so $z = 0$, we use the low induction number approximation and we are interested only in the imaginary part of the magnetic field, so we can omit the first term as a contribution to the real part.

$$\Im\left(H_z\right) = \frac{m}{4\pi}\int_0^\infty r\lambda^2\mathrm{J}_0(\lambda\rho)\,\mathrm{d}\lambda$$

We insert r from (11) which gives us an infinite progression of integrals; we will consider the j-th term:

$$\Im\left(H_z\right)^j = -\frac{m}{4\pi}\frac{\mathrm{i}\omega\mu_0\left(\sigma_{j+1} - \sigma_j\right)}{4}\int_0^\infty \mathrm{J}_0(\lambda\rho)\mathrm{e}^{-\lambda 2D_j}\,\mathrm{d}\lambda,$$

where D_j is a sum of layer thicknesses till the (j+1)-st boundary. Using identity (4) we get

$$\Im\left(H^s\right)^j = -\frac{m}{4\pi}\frac{\mathrm{i}\omega\mu_0\left(\sigma_{j+1} - \sigma_j\right)}{4\sqrt{\rho^2 + 4D_j^2}}$$

Inserting this into (7) we get a relation between apparent conductivity and partial conductivities of individual layers:

$$\sigma = \sum_j \frac{\sigma_{j+1} - \sigma_j}{\sqrt{1 + 4\left(\frac{D_j}{\rho}\right)^2}}$$

For infinitesimally thin layers we can change to a continuous variable D, which is a depth in the ground, and define the cumulative sensitivity:

$$R^{\mathrm{V}}(D,\rho) = -\frac{1}{\sqrt{4\left(\frac{D}{\rho}\right)^2 + 1}},$$

where ρ is the intercoil distance. From this we can derive the normalized sensitivity (published by McNeill), whose shape has been illustrated by graphs at the beginning of this brochure:

$$\Phi^{\mathrm{V}} = \frac{\partial R^{\mathrm{V}}}{\partial\left(\frac{D}{\rho}\right)} = \frac{4\frac{D}{\rho}}{\left[4\left(\frac{D}{\rho}\right)^2 + 1\right]^{\frac{3}{2}}}$$

Maximum of this function is at $D/\rho = 1/\sqrt{8}$, which gives the highest sensitivity in the depth of 0.35ρ.

Horizontal magnetic dipole

To obtain the apparent conductivity, we will proceed analogically to the case of vertical configuration: earth is perpendicular to the z-axis, dipole is now in the x-direction.

$$F_x^{\mathrm{2DF}}(k_x, k_y, z) = \frac{\mathrm{i}\omega\mu_0 m}{2u_0}\mathrm{e}^{-u_0 z}$$

$$\vec{H} = -(\sigma + \mathrm{i}\omega\varepsilon)\vec{F} + \frac{1}{\mathrm{i}\omega\mu_0}\nabla(\nabla\vec{F})$$

H_z obtained from $\vec{F}_X = (F_x, 0, 0)$ and $\vec{F} = (0, 0, F)$ must be equal.

$$H_z^{(x)} = \frac{1}{\mathrm{i}\omega\mu_0}\frac{\partial^2 F_x}{\partial x \partial z} = \frac{1}{4\pi}\int_{-\infty}^{\infty}\int_{-\infty}^{\infty} -\mathrm{i}k_x\frac{m}{2}\mathrm{e}^{-u_0 z}\mathrm{e}^{\mathrm{i}(k_x x + k_y y)}\,\mathrm{d}k_x\,\mathrm{d}k_y$$

$$H_z^{(z)} = \frac{1}{\mathrm{i}\omega\mu_0}\left(\frac{\partial^2}{z^2} + k_0^2\right)F^{\mathrm{2DF}} = \frac{1}{\mathrm{i}\omega\mu_0}\left(k_x^2 + k_y^2\right)F^{\mathrm{2DF}}$$

$$F^{\mathrm{2DF}} = -\frac{\mathrm{i}\omega\mu_0 m}{2}\frac{\mathrm{i}k_x}{k_x^2 + k_y^2}\left(\mathrm{e}^{-u_0 z} + r\mathrm{e}^{u_0 z}\right)$$

We perform inverse 2D Fourier transform

$$\begin{aligned} F(x, y, z) &= -\frac{\mathrm{i}\omega\mu_0 m}{8\pi^2}\int_{-\infty}^{\infty}\int_{-\infty}^{\infty}\left(\mathrm{e}^{-u_0 z} + r\mathrm{e}^{u_0 z}\right)\frac{\mathrm{i}k_x}{k_x^2 + k_y^2}\mathrm{e}^{\mathrm{i}(k_x x + k_y y)}\,\mathrm{d}k_x\mathrm{d}k_y \\ &= -\frac{\mathrm{i}\omega\mu_0 m}{8\pi^2}\int_{-\infty}^{\infty}\int_{-\infty}^{\infty}\frac{\partial}{\partial x}\left(\mathrm{e}^{-u_0 z} + r\mathrm{e}^{u_0 z}\right)\frac{1}{\lambda^2}\mathrm{e}^{\mathrm{i}(k_x x + k_y y)}\,\mathrm{d}k_x\mathrm{d}k_y \end{aligned}$$

and convert to Hankel transform

$$F(x, y, z) = -\frac{\mathrm{i}\omega\mu_0 m}{4\pi}\frac{\partial}{\partial x}\int_0^{\infty}\left(\mathrm{e}^{-u_0 z} + r\mathrm{e}^{u_0 z}\right)\frac{1}{\lambda}\mathrm{J}_0(\lambda\rho)\,\mathrm{d}\lambda \qquad (12)$$

Approximations: $k_0 = 0$, $u_0 = \lambda$, $r = \frac{\lambda - u}{\lambda + u}$; $z = 0$.

$$\begin{aligned} H_x &= \frac{1}{\mathrm{i}\omega\mu_0}\frac{\partial^2 F}{\partial x \partial z} = \frac{m}{4\pi}\frac{\partial^2}{\partial x^2}\int_0^{\infty}\left(\mathrm{e}^{-u_0 z} - r\mathrm{e}^{u_0 z}\right)\mathrm{J}_0(\lambda\rho)\,\mathrm{d}\lambda \\ &= \frac{m}{4\pi}\frac{\partial^2}{\partial x^2}\int_0^{\infty}\frac{2u}{\lambda + u}\mathrm{J}_0(\lambda\rho)\,\mathrm{d}\lambda \end{aligned}$$

Identities:

$$\frac{\partial}{\partial x} = \frac{x}{\rho}\frac{\partial}{\partial \rho}, \quad \frac{\partial \mathrm{J}_0(\lambda\rho)}{\partial \rho} = -\lambda \mathrm{J}_1(\lambda\rho)$$

$$H_x = \frac{m}{4\pi}\frac{\partial}{\partial x}\left(\frac{x}{\rho}\eta\right)$$

$$\eta = -\frac{2}{k^2}\int_0^\infty (\lambda - u)\lambda u \mathrm{J}_1(\lambda\rho)\,\mathrm{d}\lambda$$

$$= -\frac{2}{k^2}\int_0^\infty \lambda^2 u \mathrm{J}_1(\lambda\rho)\,\mathrm{d}\lambda + \frac{2}{k^2}\int_0^\infty \lambda^3 \mathrm{J}_1(\lambda\rho)\,\mathrm{d}\lambda - 2\int_0^\infty \lambda \mathrm{J}_1(\lambda\rho)\,\mathrm{d}\lambda$$

Identity:

$$\int_0^\infty \frac{\lambda}{u}\mathrm{e}^{-uz}\mathrm{J}_0(\lambda\rho)\,\mathrm{d}\lambda = \frac{\mathrm{e}^{-\mathrm{i}kr}}{r}, \quad r = \sqrt{\rho^2 + z^2}$$

$$\frac{\partial^2}{\partial z^2}\left[\frac{\partial}{\partial \rho}\int_0^\infty \frac{\lambda}{u}\mathrm{e}^{-uz}\mathrm{J}_0(\lambda\rho)\,\mathrm{d}\lambda\right]_{z=0} = \frac{\partial^2}{\partial z^2}\left[\frac{\partial}{\partial \rho}\frac{\mathrm{e}^{-\mathrm{i}kr}}{r}\right]_{z=0}$$

$$\int_0^\infty \lambda^2 u \mathrm{J}_1(\lambda\rho)\,\mathrm{d}\lambda = \frac{1}{\rho^4}\left(k^2\rho^2 - 3\mathrm{i}k\rho - 3\right)\mathrm{e}^{-\mathrm{i}k\rho}$$

Identity:

$$\int_0^\infty \mathrm{e}^{-\lambda z}\mathrm{J}_0(\lambda\rho)\,\mathrm{d}\lambda = \frac{1}{r}$$

$$\left[\frac{\partial}{\partial \rho}\int_0^\infty \mathrm{e}^{-\lambda z}\mathrm{J}_0(\lambda\rho)\,\mathrm{d}\lambda\right]_{z=0} = \left[\frac{\partial}{\partial \rho}\frac{1}{r}\right]_{z=0}$$

$$\int_0^\infty \lambda \mathrm{J}_1(\lambda\rho)\,\mathrm{d}\lambda = \frac{1}{\rho^2}$$

Identity:

$$\left[\frac{\partial^2}{\partial z^2}\frac{\partial}{\partial \rho}\int_0^\infty \mathrm{e}^{-\lambda z}\mathrm{J}_0(\lambda\rho)\,\mathrm{d}\lambda\right]_{z=0} = \left[\frac{\partial^2}{\partial z^2}\frac{\partial}{\partial \rho}\frac{1}{r}\right]_{z=0}$$

$$\int_0^\infty \lambda^3 \mathrm{J}_1(\lambda\rho)\,\mathrm{d}\lambda = -\frac{3}{\rho^4}$$

$$\eta = -\frac{2}{k^2\rho^4}\left[3 + k^2\rho^2 - \left(3 + 3\mathrm{i}k\rho - k^2\rho^2\right)\mathrm{e}^{-\mathrm{i}k\rho}\right]$$

$$\frac{\partial \eta}{\partial \rho} = -\frac{2}{k^2\rho^5}\left[-2k^2\rho^2 - 12 + \left(-\mathrm{i}k^3\rho^3 - 5k^2\rho^2 + 12\mathrm{i}k\rho + 12\right)\mathrm{e}^{-\mathrm{i}k\rho}\right]$$

$$H_x = \frac{m}{4\pi\rho^3}\left[y^2\eta + x^2\rho\frac{\partial \eta}{\partial \rho}\right]$$

Coils are coplanar, so we put $x = 0$ and $y = \rho$ (the intercoil distance).

$$H_x^s = -\frac{m}{2\pi k^2 \rho^5}\left[3 + k^2\rho^2 - \left(3 + 3\mathrm{i}k\rho - k^2\rho^2\right)\mathrm{e}^{-\mathrm{i}k\rho}\right]$$

$$H_x^p = -\frac{m}{4\pi\rho^3}$$

$$\frac{H^s}{H^p} = \frac{2}{k^2\rho^2}\left[3 + k^2\rho^2 - \left(3 + 3\mathrm{i}k\rho - k^2\rho^2\right)\mathrm{e}^{-\mathrm{i}k\rho}\right]$$

Substituing $\gamma = \mathrm{i}k$ to get McNeill's formula

$$\frac{H^s}{H^p} = \frac{2}{\gamma^2\rho^2}\left[-3 + \gamma^2\rho^2 + \left(3 + 3\gamma\rho + \gamma^2\rho^2\right)\mathrm{e}^{-\gamma\rho}\right] \tag{13}$$

Using the induction number: $B = \frac{\gamma\rho}{\sqrt{2\mathrm{i}}}$

$$\frac{H^s}{H^p} = \frac{-\mathrm{i}}{B^2}\left\{-3 + 2\mathrm{i}B^2 + \left[(3 + 3B) + \mathrm{i}\left(3B + 2B^2\right)\right]\mathrm{e}^{-B}\left(\cos B - \mathrm{i}\sin B\right)\right\}$$

Quadrature:

$$\left(\frac{H^s}{H^p}\right)_{\mathrm{q}} = -\frac{\mathrm{i}}{B^2}\left[-3 + (3 + 3B)\,\mathrm{e}^{-B}\cos B + \left(3B + 2B^2\right)\mathrm{e}^{-B}\sin B\right]$$

Taylor expansion for small B:

$$\left(\frac{H^s}{H^p}\right)_{\mathrm{q}} = \mathrm{i}\left[\frac{B^2}{2} - \frac{4B^3}{15} + \frac{4B^5}{105} - \frac{B^6}{72} + \mathcal{O}(B^7)\right]$$

For very small B:

$$\left(\frac{H^s}{H^p}\right)_{\mathrm{q}}^{\mathrm{H}} \approx \frac{\mathrm{i}B^2}{2} = \frac{\gamma^2\rho^2}{4} = \frac{\mathrm{i}\sigma\mu_0\omega\rho^2}{4}$$

This formula is typical for the linear part of the calibration curve of electromagnetic conductivity meters. With increasing induction number the second term of the expansion gives a distinct negative contribution, which results in the decreasing part of the calibration curve and ambiguous results of measurements. It is worth noticing that the negative contribution is twice smaller than in the vertical configuration, which widens the range of the linear part of the calibration curve for this configuration.

Now we can express the apparent conductivity σ^{H}:

$$\sigma^{\mathrm{H}} = \frac{4}{\mathrm{i}\mu_0\omega\rho^2}\left(\frac{H^s}{H^p}\right)^{\mathrm{H}}_{\mathrm{q}} \tag{14}$$

Now we look at the real part of (13):

$$\Re\left(\frac{H^s}{H^p}\right) = \frac{1}{B^2}\left[2B^2 - (3+3B)\mathrm{e}^{-B}\sin B + \left(3B+2B^2\right)\mathrm{e}^{-B}\cos B\right]$$

Taylor expansion for small B:

$$\Re\left(\frac{H^s}{H^p}\right) = 1 + \frac{4B^3}{15} - \frac{B^4}{6} + \frac{4B^5}{105} + \mathcal{O}(B^6)$$

For very small B:

$$\Re\left(\frac{H^s}{H^p}\right)^{\mathrm{H}} = 1 + \frac{2\sqrt{2}}{15}\left(\omega\mu_0\sigma\right)^{\frac{3}{2}}\rho^3$$

From this formula we can see that after subtraction of the primary field (number one – the first term) the most significant term contains a contribution of ground conductivity. This is undesirable effect for using in-phase to measure magnetic susceptibility. The influence of the third negative term of the Taylor expansion for bigger induction number is again smaller for horizontal configuration.

Horizontal dipole – depth-depending sensitivity

We will again proceed analogically to the vertical case, starting from equation (12):

$$F(x,y,z) = -\frac{\mathrm{i}\omega\mu_0 m}{4\pi}\frac{\partial}{\partial x}\int_0^\infty \left(\mathrm{e}^{-u_0 z} + r\mathrm{e}^{u_0 z}\right)\frac{1}{\lambda}\mathrm{J}_0(\lambda\rho)\,\mathrm{d}\lambda$$

We omit the first term, as it is only a contribution to the real part of the magnetic field.

$$\begin{aligned}\Im\left(H_x\right) &= \frac{1}{\mathrm{i}\omega\mu_0}\frac{\partial^2 F}{\partial x\partial z}\\ &= \frac{m}{4\pi\rho}\int_0^\infty r\mathrm{e}^{u_0 z}\lambda\mathrm{J}_1(\lambda\rho)\,\mathrm{d}\lambda - \frac{m}{4\pi\rho}\int_0^\infty r\mathrm{e}^{u_0 z}\mu_0\frac{x^2}{\rho^2}\lambda\mathrm{J}_2(\lambda\rho)\,\mathrm{d}\lambda\end{aligned}$$

For this configuration: $z = 0$, $x = 0$.

$$\Im\left(H_x\right) = \frac{m}{4\pi\rho}\int_0^\infty r\lambda \mathrm{J}_1(\lambda\rho)\,\mathrm{d}\lambda$$

We insert the recursive formula for reflection coefficient from a multi-layer (11). $\Im\left(H_x\right)$ becomes an infinite progression with j-th term:

$$\Im\left(H_x\right)^j = -\frac{m}{4\pi\rho}\frac{\mathrm{i}\omega\mu_0\left(\sigma_{j+1}-\sigma_j\right)}{4}\int_0^\infty \frac{\mathrm{e}^{-2D_j\lambda}}{\lambda}\mathrm{J}_1(\lambda\rho)\,\mathrm{d}\lambda$$

Identity:

$$\int_0^\infty \frac{\mathrm{e}^{-a\lambda}}{\lambda}\mathrm{J}_1(\lambda\rho)\,\mathrm{d}\lambda = \frac{\sqrt{\rho^2+a^2}-a}{\rho}$$

$$\Im\left(H_x\right)^j = -\frac{m}{4\pi\rho}\frac{\mathrm{i}\omega\mu_0\left(\sigma_{j+1}-\sigma_j\right)}{4}\frac{\sqrt{\rho^2+\left(2D_j\right)^2}-2D_j}{\rho},$$

where σ_j is conductivity of the j-th layer. Inserting this into (14) we get a relation between apparent conductivity and partial conductivities of individual layers:

$$\sigma = \sum_j \left(\sigma_{j+1}-\sigma_j\right)\frac{\sqrt{\rho^2+\left(2D_j\right)^2}-2D_j}{\rho}$$

For infinitesimally thin layers we can change to a continuous variable D, which is a depth in the ground, and define cumulative sensitivity:

$$R^{\mathrm{H}}(D,\rho) = -\frac{\sqrt{\rho^2+\left(2D\right)^2}-2D}{\rho} = 2\frac{D}{\rho}-\sqrt{1+4\left(\frac{D}{\rho}\right)^2},$$

where ρ is the intercoil distance. From this we can derive the normalized sensitivity (published by McNeill), whose shape has been illustrated in graphs at the beginning of this brochure:

$$\Phi^{\mathrm{H}} = \frac{\partial R^{\mathrm{H}}}{\partial\left(\frac{D}{\rho}\right)} = 2-\frac{4\frac{D}{\rho}}{\sqrt{4\left(\frac{D}{\rho}\right)^2+1}}$$

Maximum of this function for $D \geq 0$ is at $D/\rho = 0$, which gives the highest sensitivity at the surface.